HHS Public Access

Author manuscript

Dev Cell. Author manuscript; available in PMC 2023 February 28.

Published in final edited form as:

Dev Cell. 2022 February 28; 57(4): 480–495.e6. doi:10.1016/j.devcel.2022.01.015.

Matrix Remodeling Controls a Nuclear Lamin A/C-Emerin Network that Directs Wnt-Regulated Stem Cell Fate

Yi Tang[*,1,2], **Lingxin Zhu**[1,2], **Jung-Sun Cho**[1,2], **Xiao-Yan Li**[1,2], **Stephen J. Weiss**[*,1,2]

[1]Division of Genetic Medicine, Department of Internal Medicine, University of Michigan, Ann Arbor, MI 48109

[2]Life Sciences Institute, University of Michigan, Ann Arbor, MI 48109

Summary

Skeletal stem cells (SSCs) reside within a 3-dimensional extracellular matrix (ECM) compartment and differentiate into multiple cell lineages, thereby controlling tissue maintenance and regeneration. Within this environment, SSCs can proteolytically remodel the surrounding ECM in response to growth factors that direct lineage commitment via undefined mechanisms. Here, we report that Mmp14-dependent ECM remodeling coordinates canonical Wnt signaling and guides stem cell fate by triggering an integrin-activated reorganization of the SCC cytoskeleton that controls nuclear lamin A/C levels via the linker of nucleoskeleton and cytoskeleton (LINC) complex. In turn, SSC lamin A/C levels dictate the localization of emerin, an inner nuclear membrane protein whose ability to regulate β-catenin activity modulates Wnt signaling while directing lineage commitment *in vitro* and *in vivo*. These findings define a previously undescribed axis wherein SSCs use Mmp14-dependent ECM remodeling to control cytoskeletal and nucleoskeletal organization, thereby governing Wnt-dependent stem cell fate decisions.

eTOC

Tang et al. show that skeletal stem cells mobilize the proteolytic enzyme, MMP14, to remodel their surrounding extracellular matrix in order to activate a β1 integrin signaling axis that controls canonical Wnt signaling and lineage commitment via the regulation of a nuclear lamin A/C-emerin- β-catenin network.

Graphical Abstract

[*]**Corresponding Authors:** Stephen J. Weiss, MD, sjweiss@umich.edu, Life Sciences Institute, Mary Sue Coleman Hall, University of Michigan, 210 Washtenaw, Ann Arbor, MI 48109-2216, Yi Tang, PhD, yitang@umich.edu, Life Sciences Institute, Mary Sue Coleman Hall, University of Michigan, 210 Washtenaw, Ann Arbor, MI 48109-2216.

Lead Contact: Stephen J. Weiss, MD, sjweiss@umich.edu, Life Sciences Institute, Mary Sue Coleman Hall, University of Michigan, 210 Washtenaw, Ann Arbor, MI 48109-2216

Author Contribution

Y.T., S.J.W. designed experiments, Y.T., L.Z., J-S.C., X-Y.L. performed experiments, Y.T., L.Z., J-S.C., X-Y.L., S.J.W. analyzed data, Y.T., S.J.W. conceived and oversaw the project, Y.T., S.J.W. wrote and edited the manuscript.

Competing interests: The authors declare no competing interests.

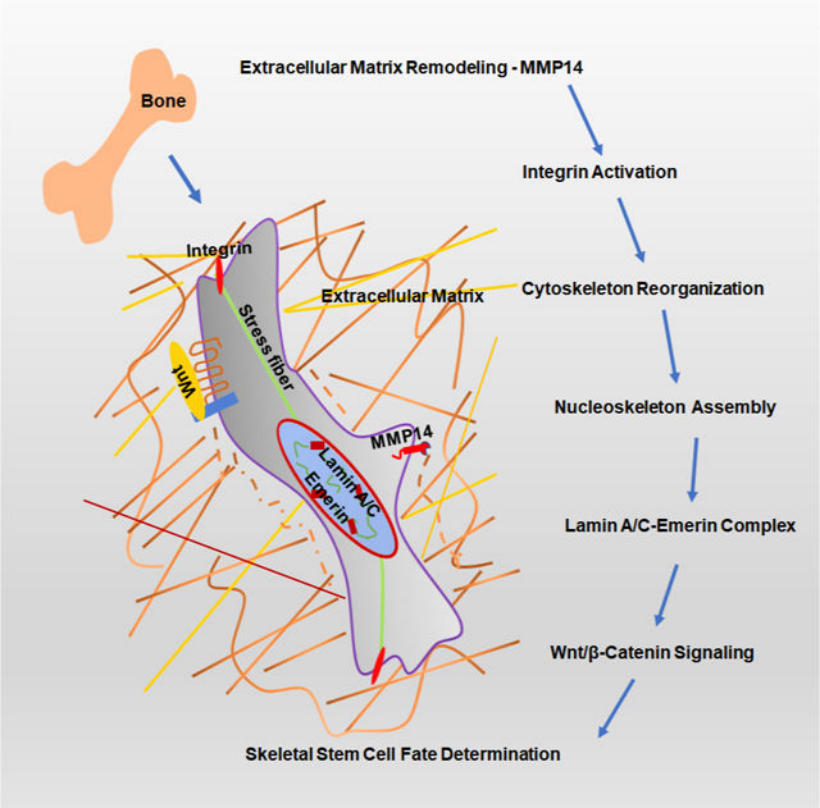

Introduction

Skeletal stem cells (SSCs) play key roles in regulating skeletal hemostasis as well as supporting hematopoiesis in health and disease (Baron and Kneissel, 2013; Baryawno et al., 2019; Ono et al., 2019; Serowoky et al., 2020). In this regard, SSC can activate differentiation programs that allow for their alternative commitment to either osteoblast, adipocyte or chondrocyte lineages – a fate decision process that falls under the control of canonical Wnt signaling (Baron and Kneissel, 2013; Baryawno et al., 2019; Murphy et al., 2020; Ono et al., 2019; Serowoky et al., 2020). During lineage commitment, SSCs interface with a 3-dimensional (3D) extracellular matrix (ECM) that controls cell differentiation and fate (Smith et al., 2018; Walma and Yamada, 2020). While the structure, topology, and biomechanical properties of the ECM directly impact stem cell function (Chaudhuri et al., 2020; Walma and Yamada, 2020), the ECM is a dynamic scaffold that is actively remodeled as a function of pericellular proteolysis (Chun et al., 2006; Feinberg et al., 2018; Tang et al., 2013; Zhu et al., 2020).

In 2D culture, cell shape changes trigger the reorganization of cytoskeletal architecture, an event that potentially impacts nuclear structure and transcription by transducing mechanical signals via an interacting set of proteins known as the linker of nucleoskeleton and cytoskeleton (LINC) complexes that, in turn, establish binding interactions with nuclear lamin A and C (Kirby and Lammerding, 2018; Lele et al., 2018). By contrast, how 3D SSC shape changes evolving as a consequence of ECM remodeling impact nuclear structure

and stem cell fate – *in vitro* or *in vivo* – remains undefined. Herein, we demonstrate that ECM remodeling regulates both canonical Wnt signaling and SSC lineage commitment by modulating the LINC-dependent control of nuclear lamin A/C levels, β-catenin nuclear translocation and co-transcriptional activity.

Results

Mmp14-dependent ECM remodeling Regulates SSC Canonical Wnt Signaling

To recapitulate an *in vivo*-like environment *in vitro*, an enriched population of bone marrow SSCs/progenitors were isolated from wild-type mice and cultured in 3D within soft, native cross-linked hydrogels of type I collagen with a fibril stiffness of approximately 50 *Pa* (Feinberg et al., 2018; Tang et al., 2013). Under these conditions, SSCs rapidly spread and change cell shape by hydrolyzing pericellular collagen fibrils as detected with an antibody specific for cleaved collagen fragments (Ferrari et al., 2019) (Figure 1A). While type I collagen is resistant to most forms of proteolytic attack, it can be degraded by a subset of collagenolytic enzymes belonging to the matrix metalloproteinase (MMP) gene family (Feinberg et al., 2018). Indeed, when collagen-embedded wild-type SSCs are cultured in the presence of the broad-spectrum MMP inhibitor, BB-94 (Fields, 2019), collagenolytic activity is largely lost (Figure 1A), and the SSCs are unable to undergo their normal 3D shape change and assume more rounded shapes with dendritic-like extensions (Figure S1A and S1B). Given that the dominant type I collagenolytic proteinase found in mammals is the type I transmembrane MMP, MMP14 (Chun et al., 2006; Feinberg et al., 2018; Tang et al., 2013; Zhu et al., 2020), we isolated SSCs from *Mmp14*$^{-/-}$ mice and cultured them in collagen hydrogels. Under these conditions, collagenolytic activity is largely, but not completely, lost (Figure 1A) as knockout SCCs upregulate other type I collagenases, including *Mmp13* and *Mmp15* by 10.3 and 1.6 -fold, respectively (n=2). Nevertheless, the 3D cell shape changes normally observed in wild-type SSCs are blocked in Mmp14-null cells (Figure S1A and S1B). As cell shape modulates gene expression (Alisafaei et al., 2019), mRNA was harvested from collagen-embedded wild-type and *Mmp14* knockout cells after a 48 h culture period to screen for transcriptional changes. Consistent with earlier work, alterations in Hippo signaling were observed (Tang et al., 2013), but among the more than 1500 changes in gene expression detected (using a 1.5-fold cutoff and a $p < 0.05$), DAVID analysis highlighted major alterations in canonical Wnt signaling [ranging from marked downregulation of Wnt antagonists (e.g., *Axin2*, *Dkk2* and *Notum*), Wnt receptors and ligands (*Fzd1*, *Fzd7* and *Wnt10b*) to the upregulation of Wnt signaling modulators (e.g., *Srfp2*, *Rspo2* and *Rspo3*)], a network critical to directing SSC lineage commitment to osteogenesis as opposed to adipogenesis (Chen and Long, 2013; Day et al., 2005; Matsushita et al., 2020) (Figure 1B, Figure S1C). Classically, cells stimulated with a canonical Wnt ligand, such as Wnt-3a, stabilize β-catenin protein levels by preventing its constitutive phosphorylation and subsequent proteasomal degradation (Clevers and Nusse, 2012). In turn, following its nuclear translocation, β-catenin acts as a transcriptional co-activator by binding to transcription factors belonging to the TCF/LEF family (Clevers and Nusse, 2012). Consistent with this model, collagen-embedded, wild-type SSCs respond to Wnt-3a stimulation by increasing protein levels of active (i.e., non-phosphorylated) β-catenin and shuttling the protein into the nuclear compartment (Figures 1C and 1D). By

contrast, when Mmp14-null SSCs are cultured under 3D conditions with Wnt-3a, increases in active β-catenin levels are blunted along with a block in nuclear translocation (Figures 1C and 1D). Consequently, expression of downstream targets of β-catenin-TCF/LEF-dependent transcription, e.g., *Axin2*, *Dkk2* and *Tcf7* (Chen and Long, 2013), though increased in wild-type SSCs, are repressed significantly in Mmp14-null cells (Figure 1E). As decreased β-catenin/Wnt signaling promotes an adipogenic fate over osteogenesis (Chen and Long, 2013; Day et al., 2005; Matsushita et al., 2020), we also find that 3D culture of Mmp14-null SSCs preferentially skews the cells towards adipogenesis (Figure S1D and S1E). Osteogenic commitment in Mmp14-null SSCs could, however, be rescued by transducing cells with a constitutively active S33Y β-catenin mutant (Yook et al., 2006) (Figures S1F–S1I). Of note, the required role for Mmp14 in optimizing Wnt responses is strictly confined to 3D culture, i.e., when wild-type or null SSCs are stimulated with Wnt-3a under standard 2D conditions, a scenario where collagenolytic activity is not required to support cell shape changes, β-catenin levels increase comparably in both cell populations in tandem with expected increases in *Axin2*, *Dkk2* and *Tcf7* expression (Figures 1F and 1G). Likewise, under these conditions, osteogenic and adipogenic potential are unaffected (Figures S1J and S1K). Finally, to determine the degree to which osteogenic defects observed in 3D culture *in vitro* match the *in vivo* setting, we examined canonical Wnt signaling in the calvarium, a region enriched in SSCs (Zhao et al., 2015), of newborn wild-type vs *Mmp14*$^{-/-}$ mice. Indeed, non-phosphorylated β-catenin levels are downregulated significantly in *Mmp14*$^{-/-}$ mice as assessed by immunostaining or Western blot analysis in concert with decreases in *Axin2*, *Dkk2* and *Tcf7* expression *in vivo* (Figures 1H–1K).

An Integrin-Cytoskeletal Axis Regulates Canonical Wnt Signaling

Mmp14-dependent regulation of SSC shape occurring as a consequence of collagenolytic activity correlates with changes in Wnt signaling, but collagen degradation products themselves potentially exert bioactive effects (Wells et al., 2015). Further, the substrate spectrum of the proteinase is known to extend beyond type I collagen (Tang et al., 2013; Feinberg et al., 2018), raising the possibility that the metalloproteinase hydrolyzes other cell-associated or secreted targets that impact Wnt signaling. As such, to determine whether Mmp14-dependent cell shape changes directly underlie Wnt responsiveness, wild-type SSCs were alternatively cultured within a polyethylene glycol (PEG)-based, Arg-Gly-Asp (RGD) integrin ligand-decorated, synthetic hydrogel whose crosslinks do – or do not – harbor an Mmp14-cleavable peptide bond (Ehrbar et al., 2011; Tang et al., 2013) (Figure 2A). In the presence of Wnt-3a, wild-type SSCs embedded in hydrogels with Mmp14-sensitive crosslinks undergo the expected 3D shape changes and increase active β-catenin levels as well as β-catenin-TCF/LEF-dependent transcription (Figures 2B, 2C and S2A). By contrast, when wild-type SSCs are cultured in the Mmp14-resistant hydrogel, cell shape changes are blocked and the cells remain insensitive to Wnt-3a stimulation (Figures 2B, 2C and S2A). Hence, the Mmp14-null phenotype is recapitulated when wild-type SSCs are incapable of degrading the synthetic matrix, thereby precluding the required 3D cell shape changes.

To define the underlying mechanisms that link SSC 3D shape changes to Wnt signaling, we focused on potential interactions between ECM remodeling and cytoskeletal reorganization (Kirby and Lammerding, 2018; Lele et al., 2018). In 3D culture, wild-type, but not Mmp14-

null SSCs, activate β1 integrin, a major receptor subtype responsible for binding type I collagen (Chaudhuri et al., 2020) (Figures 2D and S2B). Coincident with β1 integrin activation, F-actin levels increases are detected in wild-type, but not *Mmp14*$^{-/-}$ SSCs in 3D collagen culture (Figure 2E and S2C). Similarly, when wild-type SSCs are embedded in the Mmp14-sensitive PEG hydrogels, F-actin assembly increases, a response not observed in the MMP-resistant PEG hydrogel (Figures 2F and S2D). By contrast, Mmp14-null SSCs are able to organize F-actin normally in standard 2D culture, ruling out an intrinsic cytoskeletal defect in the knockout cells (Figures 2G and S2E). Underlining the importance of integrin activation and actin polymerization, wild-type SSCs decrease their ability to respond to Wnt-3a when cultured in the presence of either a blocking antibody directed against β1 integrin or an inhibitor of actin polymerization, i.e., cytochalasin D (Figures 2H–2N, S2F and S2G). The defects in F-actin organization and Wnt signaling inherent to *Mmp14*$^{-/-}$ SSCs are, however, reversed following transduction with a constitutively activated β1 integrin mutant (G429N) (Paszek et al., 2005) (Figures 2O–2Q and S2H). Hence, Mmp14-dependent ECM remodeling plays a required role in activating a β1 integrin/F-actin cascade necessary to support canonical Wnt signaling.

Mmp14-Dependent ECM Remodeling Controls Nuclear Lamin A/C Levels

Activated integrins interacting with the F-actin cytoskeleton are able to transmit mechanical signals directly to the nucleus via a family of cytoskeleton-binding proteins, termed nesprins, whose C-terminal tail pass through the outer nuclear membrane where they bind to a second family of transmembrane proteins, the SUN proteins (Kirby and Lammerding, 2018; Lele et al., 2018). In turn, SUN proteins pass through the inner nuclear membrane where their nucleoplasmic tail binds to the nucleoskeletal intermediate filament proteins, lamins A and C (alternate splice products of a single *Lmna* gene) (Kirby and Lammerding, 2018; Lele et al., 2018). Together, the nesprin/SUN complex, abbreviated as the linker of nucleoskeleton and cytoskeleton or LINC complexes, allows cytoskeletal-generated forces to impact nuclear shape, organization and function (Kirby and Lammerding, 2018; Lele et al., 2018). In 3D culture, wild-type and Mmp14-null SSCs display similar subcellular distributions of nesprins 1 and 2 as well as Sun1 (Figures S3A–S3C). However, while wild-type SSC nuclei display ovoid shapes with lamin A/C proteins localized to both the nuclear envelope and nucleoplasm, both nuclear shape and lamin A/C levels are notably altered in either *Mmp14*$^{-/-}$ SSCs or wild-type SSCs cultured with BB-94 (Figure 3A). Further, the decrement in lamin A/C immunostaining observed in 3D-embedded, Mmp14-null or BB-94-inhibited wild-type SSCs coincides with decreases in lamin A/C protein (but not mRNA) levels as assessed by Western blot in tandem with increases in phospho-lamin A/C, a post-translational modification of lamin A/C that can promote its degradation (Buxboim et al., 2014; Swift et al., 2013) (Figure 3B). By contrast, lamin B1 and B2, members of the lamin B family whose distribution is confined to the nuclear lamina (Kirby and Lammerding, 2018; Lele et al., 2018), are unchanged in Mmp14-null SSCs (Figures 3C–3D and S3D). Finally, as observed for Wnt signaling, Mmp14-dependent changes in cell shape are also linked directly to the observed alterations in lamin A/C levels, i.e., lamin A/C and phospho-lamin A/C levels are up- or down- modulated, respectively, when wild-type SSCs are alternatively cultured in Mmp14-sensitive vs insensitive PEG hydrogels (Figure 3E, 3F and S3E). However, when wild-type or null SSCs are cultured under standard 2D

conditions, lamin A/C distribution and protein levels are indistinguishable between the two cell populations (Figures S3F–S3H).

ECM Turnover Regulates Wnt Signaling Via the LINC Complex Assembly Network

To determine whether LINC complexes serve as a necessary intermediary coordinating changes in F-actin-dependent mechanotransduction with effects on the lamin A/C network, wild-type SSCs were next transduced with either a dominant-negative KASH (DNKASH) construct that acts as a competitive inhibitor of perinuclear interactions between endogenous nesprins and SUN family members or a DNKASH-PPPL construct where the last 4 amino acids of the KASH domain (i.e., PPPL) have been removed, thereby abolishing Sun protein interactions (Kirby and Lammerding, 2018; Zhang et al., 2019). Following transduction of wild-type SSCs with the dominant-negative construct, F-actin organization is disrupted in tandem with marked changes in nuclear shape as well as notable changes in lamin A/C distribution and attendant decreases in lamin A/C protein levels and increases in phospho-lamin A/C that recapitulate those observed in Mmp14-null cells (Figures 3G–I and S3I). DNKASH-transduced cells are also blunted in Wnt-3a responses as assessed by decreases in active β-catenin levels and nuclear translocation (Figures 3J, 3K and S3J–3L). Similar effects on lamin A/C are observed in the presence of anti-β1 integrin blocking antibodies or cytochalasin D (Figures S3M–S3Q). As these results support a model wherein the constitutively active β1 integrin mutant rescues Wnt signaling in Mmp14-null SSCs via a LINC-dependent process (Figure 2O–2Q), *Mmp14*$^{-/-}$ SSCs expressing the G429N β1 integrin mutant were transduced with the DNKASH-PPPL or DNKASH expression vectors. As predicted, DNKASH, but not DNKASH-PPPL, blocked the ability of the β1 integrin mutant to rescue Wnt signaling or lamin A/C levels in Mmp14 knockout SCCs (Figures 3L–3N, and S3R). Hence, ECM remodeling triggers β1 integrin activation, cytoskeletal reorganization and the LINC complex-mediated modulation of lamin A/C levels that together control Wnt signaling. We also note that lamin A/C levels are similarly decreased in *Mmp14*$^{-/-}$ calvaria *in vivo* along with increases in phospho-lamin A/C levels (Figures 3O, 3P and S3S).

Lmna Conditional Knockout SSCs Phenocopy Mmp14$^{-/-}$ Defects in Wnt Signaling

To assess the ability of SSC Lamin A/C levels to modulate Wnt signaling *in vivo*, mice bearing floxed lamin A genes (*Lmna*$^{f/f}$) (Kim and Zheng, 2013) were crossed with a *Dermo1/Twist2-Cre* transgenic line that allows for the global targeting of SSCs (Day et al., 2005; Tang et al., 2021; Tang et al., 2013). While conditional knockout mice are born in normal Mendelian frequency, the mice display a runted phenotype accompanied by osteopenia and decreases in bone volume, trabecular number and thickness with increases in trabecular separation (Figures 4A and S4A–S4E) as well as osteoclast numbers (Figures 4B and 4C). Defects in calvarial osteogenesis with wider sutures (Figure 4D) are found along with decreases in active β-catenin levels as well as *Axin2*, *Dkk2* and *Tcf7* expression (Figure 4E–G). Importantly, the observed defects in osteogenesis are accompanied by increased levels of bone marrow adipogenesis at both the histologic and gene expression levels (Figures 4H and 4I), hallmarks of an SSC-specific loss in canonical Wnt signaling (Song et al., 2012).

To assess the impact of Lmna targeting *in vivo* on SCC function, $Lmna^{+/+}$ and $Lmna^{-/-}$ SSCs were isolated and expanded *in vitro* and exposed to Wnt-3a in 3D culture. Whereas $Lmna^{+/+}$ SSCs increase levels of active β-catenin as well as nuclear β-catenin in response to Wnt-3a (Figure 4J–4M), $Lmna^{-/-}$ SSCs - despite retaining normal collagenolytic activity (Figures S4F and S4G), cell shape changes (Figure S4H), F-actin organization (Figure S4I), and contractile activity in 3D culture (Figure S4J and S4K) - display only minimal increases in active β-catenin levels as well as a blunted ability to translocate β-catenin into the nuclear compartment (Figures 4J–4M). Further, Axin2, *Dkk2* and *Tcf7* expression are decreased by 60–70% in $LmnA^{-/-}$ SSCs (Figure 4N). A switch in SSC lineage commitment similar to that found *in vivo* is likewise observed in 3D culture where $LmnA^{-/-}$ SSCs preferentially commit to adipogenesis versus osteogenesis (Figures S4L and S4M).

Interfacing the Lamin A/Emerin Axis with ECM Remodeling-Dependent Wnt Signaling

Nuclear lamina-associated lamin A/C controls the localization of the inner nuclear membrane protein, emerin (Sullivan et al., 1999). In the absence of lamin A/C, emerin is no longer confined to the nuclear membrane and instead, diffuses within the ER membrane (Sullivan et al., 1999; Vaughan et al., 2001) (Figures 5A and S5A). In this regard, while $Mmp14^{+/+}$ SSCs localize the bulk of their emerin to the nuclear envelope when cultured in 3D collagen, $Mmp14^{-/-}$ SSCs cultured in 3D (but not 2D) redistribute emerin to the ER despite unchanged protein levels (Figures 5B and S5B–S5G).

As emerin is able to bind β-catenin (Markiewicz et al., 2006), we considered the possibility that redistributed emerin inappropriately leads to the mislocalization of emerin/β-catenin complexes that interfere with β-catenin nuclear translocation and Wnt signaling. Indeed, while nuclear β-catenin levels are decreased in both $Lmna^{-/-}$ and $Mmp14^{-/-}$ SSCs, the formation of stable emerin/β-catenin complexes is increased in both cell populations (Figures 5C and 5D). To determine whether mislocalized emerin serves as a dominant-negative inhibitor of canonical Wnt signaling, we silenced emerin expression in $Mmp14^{-/-}$ SSCs in 3D culture with either of 2 distinct siRNA constructs. Under these conditions, active β-catenin levels increase markedly in response to Wnt-3a along with increases in β-catenin/TCF-LEF target gene expression (Figures 5E–5G). The mislocalization of emerin observed in $Mmp14^{-/-}$ SSCs and the subsequent trapping of β-catenin in emerin complexes is reversed by increasing lamin A/C expression in Mmp14-null SSCs whereupon emerin is redirected to the nuclear envelope while restoring nuclear β- catenin translocation and increasing *Axin2*, *Dkk2* and *Tcf7* expression (Figures 5H–K). Consistent with a gatekeeper function for emerin in regulating Wnt signaling, when emerin-null SSCs are cultured in 3D collagen, active β-catenin levels, nuclear β-catenin translocation and Wnt signaling are increased relative to wild-type cells (Figures S5H–S5L). Further, as lamin A overexpression increases Wnt signaling in SSCs (Bermeo et al., 2015), we sought to determine whether this effect is emerin-dependent. Indeed, whereas the forced expression of lamin A increases active β-catenin levels in $Emd^{+/+}$ SSCs, further increases in active β-catenin protein levels are not observed in $Emd^{-/-}$ SSCs (Figures 5L–5N).

Taken together, these results raise the possibility that increasing lamin A/C levels would alone restore their osteogenic potential of Mmp14-null SSCs *in vitro* and *in vivo*. As shown,

following *Lmna* transduction, Mmp14-null SSCs recover their osteogenic potential while decreasing adipogenic activity (Figures S5M and S5N). To assess lineage commitment *in vivo*, $Mmp14^{+/+}$ SSCs or $Mmp14^{-/-}$ SSCs were transduced with either a control or *Lmna* expression vector, embedded in type I collagen plugs and transplanted into recipient mice (Figure 5O). While cell-free collagen plugs do not support osteogenesis or adipogenesis, wild-type SSCs responding to endogenously-derived Wnt signals commit to osteogenesis and generate bone (Figures 5O and S5O). By contrast, control vector-transduced $Mmp14^{-/-}$ SSCs preferentially differentiate into adipocytes and fail to generate ectopic bone (Figures 5O and S5O). Remarkably, however, following *Lmna* expression, the Mmp14-null SSCs suppress adipogenic commitment and regain an osteogenic potential comparable to wild-type cells (Figures 5O and S5O).

Finally, confirming that conclusions based on murine SSCs can be extended to human bone marrow-derived multipotent stromal/stem cells (hMSCs), inhibiting MMP activity in 3D collagen cultures likewise blocks cell shape changes in tandem with the loss of ECM degradation while decreasing lamin A/C levels, delocalizing emerin and preventing nuclear β-catenin translocation and Wnt target gene expression (Figures S6A–S6L). Further, in the absence of MMP activity, transducing hMSCs with an *LmnA* expression vector alone restores emerin nuclear localization as well as responses to Wnt signaling (Figures S6M–S6O). However, when hMSCs are transduced with a lamin A mutant that cannot interact with emerin (Holt et al., 2003), the ability to rescue emerin nuclear localization and Wnt signal transduction is lost (Figures S6M–6O).

Mmp14 Activity Directs the SSC Osteogenic/Adipogenic Switch

Under the conditions examined thus far, 3D matrix-embedded SSCs either commit to osteogenesis when Mmp14 is fully active or to adipogenesis when Mmp14 activity is ablated. However, these results beg the question as to whether wild-type SSCs purposefully autoregulate Mmp14 activity when differentially stimulated under osteogenic versus adipogenic conditions. To this end, SSCs were cultured within collagen hydrogels and alternatively stimulated to undergo osteogenesis or adipogenesis in order to track Mmp14-dependent changes in lamin A/C, emerin localization and Wnt signaling activity. During osteogenesis, SSCs in 3D culture assemble a prominent F-actin network surrounding ovoid-shaped, lamin A/C-rich nuclei while expressing high levels of Mmp14 (Figures 6A–6E). By contrast, SSCs undergoing adipogenesis, display only low levels of F-actin that circumscribe buckled, spheroid-shaped nuclei with only low levels of Mmp14 and lamin A/C evident (Figures 6A, 6B, and 6F–6H). Coincident with these divergent differentiation programs, emerin retains its nuclear localization during osteogenesis in tandem with β-catenin nuclear translocation and increased *Axin2* expression (Figures 6I–6M). In contradistinction, adipogenesis triggers the redistribution of emerin away from the nuclear envelope with the tandem down-regulation of nuclear β-catenin levels and transcriptional activity (Figures 6I–6M). Taken together, these studies identify Mmp14-dependent remodeling of the SSC pericellular ECM as the master regulator of canonical Wnt signaling via the LINC-mediated control the lamin A/C/emerin network (Figure 7).

Discussion

Herein, we report that the proteolytic remodeling of the pericellular ECM is a required determinant of canonical Wnt signaling *in vitro* and *in vivo*. Recent studies have demonstrated that cells modulate both lamin A/C levels and their distribution between the nuclear lamina and the nucleoplasmic pools as a function of changes in ECM rigidity (Buxboim et al., 2014; Heo et al., 2016; Smith et al., 2018; Swift et al., 2013). Our studies, however, uncover a key auto-regulatory loop wherein SSCs directly control their lamin A/C levels in a cell-autonomous fashion via Mmp14-dependent ECM remodeling. While MMPs have been reported to play a role in degrading lamin A/C itself following a decrease in matrix-dependent mechanosensing (Cho et al., 2019), we find that lamin turnover proceeds in the absence of MMP activity when matrix remodeling is inhibited. Interestingly, the identification of lamin A/C as a downstream target of Mmp14-dependent ECM remodeling is highlighted by the overlapping phenotypes observed in *Mmp14*$^{-/-}$ and *Lmna*$^{-/-}$ mice where each undergo normal embryonic development, but display rapid-onset, postnatal morbidities associated with similar defects in bone, fat, muscle and cardiac development that coalesce into premature mortality by 2–3 months of age (Holmbeck et al., 1999; Li et al., 2011; Nikolova et al., 2004; Sullivan et al., 1999; Tang et al., 2013). Interestingly, while the loss of Wnt signaling and the switch to adipogenic commitment are commonly viewed as default states, changes in transcriptional programming are, in fact, more dramatic when SSCs undergo adipogenesis, highlighting the complexity of stem cell responses (Rauch et al., 2019; Rauch and Mandrup, 2021).

In linking canonical Wnt-initiated β-catenin signaling to Mmp14-dependent changes in lamin A/C levels, we noted that emerin's normal positioning in the inner nuclear membrane is dictated by its non-covalent interactions with lamin A/C in the nuclear lamina (Sullivan et al., 1999; Vaughan et al., 2001). Changes in nuclear lamin A/C levels can, under some conditions, also affect nesprin localization, and nuclear membrane-associated nesprins have been reported to regulate β-catenin trafficking (Neumann et al., 2010; Uzer et al., 2018). Nevertheless, underlining the functional significance of β-catenin/emerin complexes in suppressing Wnt signaling, targeting emerin alone restored canonical Wnt activity in *Mmp14*$^{-/-}$ SSCs. While other studies have identified mechanotransduction-linked, but distinct, roles for emerin in regulating cell function *in vitro* (Guilluy et al., 2014; Ho et al., 2013; Le et al., 2016), emerin-null mice display few pathologic phenotypes save for those associated with hyperactive Wnt signaling *in vivo* (Stubenvoll et al., 2015). We have previously reported that Mmp14 triggers nuclear trafficking of the Hippo effectors, YAP and TAZ (Tang et al., 2013), but interestingly, we find in unpublished work that canonical Wnt ligands can themselves trigger YAP nuclear translocation where it may function as a chaperone to control nuclear β-catenin levels and Wnt activity (Pan et al., 2018). Unraveling these intertwined networks will be the focus of future studies.

Limitations of the study

While our studies are confined to analyses of mouse as well as human bone-derived stromal stem/progenitors, we posit that other stem cell populations, including those of neoplastic origin, that reside in collagen-rich tissue such as those found in the perivascular niche of

lung, muscle or fat (Jones and Wagers, 2008), may likewise use Mmp14 to remodel their pericellular ECM in order to coordinate Wnt signaling and stem cell fate. Further study is also needed to determine whether a critical role for this axis may also extend to the laminopathies where changes in *MMP14* levels and ECM expression occur in tandem with defects in Wnt signaling (Csoka et al., 2004; Hernandez et al., 2010). Finally, we note that remodeling nuclear lamin A/C levels also controls the localization of additional inner nuclear membrane proteins, including MAN1 and LAP2, molecules known to play active roles in modulating SMAD and Gli activities (Mirza et al., 2019; Pan et al., 2005). As such, ECM remodeling may well extend its control beyond Wnt signaling and the Hippo network to include TGFβ and Hedgehog signaling pathways, subjects deserving of further study.

Star * Methods

RESOURCE AVAILABLITY

Lead contact—Further information and requests for resources and reagents should be directed to and will be fulfilled by the lead contact.

Material availability—All unique materials and reagents generated in this study are available from the Lead Contact upon request.

Data and code availability

- All data reported in this paper will be shared by the lead contact upon request.
- This paper does not report original code.
- Any additional information required to reanalyze the date reported in this work paper is available from the Lead Contact upon request.

EXPERIMENTAL MODEL AND SUBJECTS DETAILS

Mice—*Mmp14*$^{+/-}$ mice (Swiss Black background), were obtained from the NIH (Holmbeck et al., 1999) and mated to generate *Mmp14*$^{-/-}$ and *Mmp14*$^{+/+}$ mice. *Lmna*$^{f/f}$ mice were provided by Yixian Zheng (Carnegie Institution for Science) and crossed into C57BL/6 mice for more than six generation (Kim and Zheng, 2013). *Lmna*$^{+/-}$ and *Dermo1-Cre* knock-in mice were obtained from the Jackson Laboratory (Maine, USA). Emd$^{-/-}$ mice were provided by Howard J. Worman (Columbia University). Nu/Nu mice were from Charles River Laboratories International, Inc. All mouse work was performed with IACUC approval.

Cell lines—Human mesenchymal stem cells (bone marrow-derived) were obtained from Sigma-Aldrich or Lonza and cultured as described below.

METHOD DETAILS

RNA Isolation and Gene Expression Analysis—Total RNA from neonatal skulls, femurs or cell cultures was harvested with TRIzol reagent (Invitrogen) and further purified with QIAGEN RNeasy Mini-kit columns (QIAGEN) following the manufacturer's direction. RNA samples were used for cDNA synthesis and amplification by real-time PCR (RT-PCR) according to the manufacturer's instructions (Power SYBR Green, Applied Biosystems).

For cells cultured in 3D collagen, the gels were disrupted and homogenized using the TissueRuptor (QIAGEN) and total RNA extracted and purified by a QIAGEN RNeasy Fibrous Tissue Mini kit. Gene expression was profiled with Affymetrix Mouse Gene 2.1 ST expression array at the University of Michigan Microarray Core. Expression values for each probe set were calculated using a robust multi-array average (RMA) and filtered for genes with a greater than 1.5-fold change. Functional annotation clusters of the changed genes were analyzed with DAVID Bioinformatics Resource 6.8 software. To analyze the RT-PCR data, raw data (CT) were obtained by PCR, and the ΔΔCT method (ΔΔCT=ΔCT (experimental gene) – ΔCT (controlled gene)) was used to calculate the relative fold of gene expression (fold=$2^{\Delta\Delta CT}$). ΔCT was calculated using housekeeping gene (Gapdh) and averaged ($\Delta CT=CT_{GAPDH}-CT_{gene}$). Three independent experiments were performed, and the means of three experiments were compared with statistical analysis. Otherwise, the number of experiments preformed is shown in the figure legends.

Cell Culture—3–5 wk-old mice femur and tibia specimens were dissected and cleaned from surrounding tissue, cut into pieces and digested with 3 mg/ml collagenase for 60 min at 37°C with constant agitation. Single-cell suspensions were collected after passing through a 40 μm cell strainer (BD Bioscience) and incubated in plastic dishes with DMEM supplemented with 10% fetal bovine serum. After 2 d of culture, cells were washed twice with PBS and the adherent cells further cultured in DMEM supplemented with 10% fetal bovine serum for an additional 3 days. The adherent colonies were then sorted by flow cytometry with antibodies to Sca-1, CD29, CD45 and CD11b as described (Tang et al., 2013). To further deplete hematopoietic cell and endothelial cell populations from the cultures, cell suspensions were incubated with Biotin anti-mouse CD34, CD45, CD11b, Ter-119, CD31 antibodies, and hematopoietic cell as well as endothelial cell lineages captured with Invitrogen MagniSort Streptavidin Negative Selection Beads according to the manufacturer's instructions. The purified cells isolated from CFU-Fs were used as SSCs. Human mesenchymal stem cells (bone marrow-derived) were obtained from Sigma-Aldrich and cultured in human mesenchymal-XF expansion medium. Human Mesenchymal Stem Cells obtained from Lonza were cultured with the mesenchymal stem cell growth medium provided by Lonza.

For 3D culture, 5×10^5 cells per ml were embedded into 2.16 mg/ml rat tail-derived type I collagen gels (Tang et al., 2013) and cultured in 24-well plates. To prepare the PEG-based hydrogel cultures, 2×10^5 cells per ml were mixed with hydrogel solution and cultured according to the manufacturer's instructions (Qgel SA). For 2D culture, SSCs were cultured at low density atop tissue culture plastic or glass slides in 6-well-dishes (1×10^4 cells/well). To activate canonical Wnt signaling, SSCs were cultured in DMEM supplemented with 1% fetal bovine serum overnight followed by the addition of 100 ng/ml recombinant Wnt-3a (R&D systems). To inhibit MMP activity, SSCs were cultured in the presence of 5 μM BB-94 as described (Feinberg et al., 2018).

***In Vitro* SSC Differentiation—**For *in vitro* experiments, 5×10^5 SSCs/well were either cultured in 6-well plates or 1×10^6 cells per ml embedded into 2.16 mg/ml rat tail-derived type I collagen gels, and 0.5 ml of the collagen-cell mixtures cultured in each well of 24-

well plates. 24 hr later, culture medium was changed and the cells induced with osteogenic medium [50 μM ascorbic acid, 10 nM dexamethasone, 10 mM β-glycerolphosphate and 2% fetal bovine serum (FBS) in low-glucose DMEM] or adipogenic medium [1 μM dexamethasone, 50 μM indomethacin, 500 nM IBMX, 5 μg/ml insulin and 2% FBS in low-glucose DMEM] (Tang et al., 2013). Differentiated cells were fixed with 4% paraformaldehyde in PBS and stained for either alkaline phosphatase (Alp) activity or Alizarin Red S in osteogenic cultures and Oil Red O for monitoring adipogenesis (Tang et al., 2013).

Immunofluorescence—Cells cultured in collagen gel or in other hydrogels were fixed with 4% paraformaldehyde for 15 min at room temperature, washed and incubated with a fresh aliquot of 4% paraformaldehyde for an additional 15 min fixation at room temperature. The cell cultures were then washed 3 times with PBS, 15 min each at room temperature. The collagen gel and the PEG-based hydrogel were then removed from the culture dish, cut into pieces, and permeabilized (0.3% Triton X-100 in PBS) for 30 min at room temperature. Cells cultured atop 2D glass surfaces were fixed with 4% paraformaldehyde for 15 min at room temperature, permeabilized (0.3% Triton X-100 in PBS) at room temperature for 15 min. All the cell cultures were then blocked (5% BSA in PBS with 0.05% Tween-20) and incubated with primary antibodies at 4°C overnight. All primary antibodies were used at a 1:200 dilution. The stained 3D cultures were mounted on glass slides and covered with a glass coverslip. For frozen sections, cell permeabilization and antibody incubations were performed under conditions identical to those used for 2D cultures as described above.

Microscopy and image analysis—Phase contrast images were acquired on an Eclipse Ts100 (Nikon Instruments). Immunofluorescence images were captured with a Leica confocal microscope. Z-stack images were collected for image reconstruction. To analyze cell shape changes in 3D cultures, phase contrast images were taken, 100 cells from five different fields were counted, and the percentage of the cells with spindle, dendritic or urchin-like shapes (depicted in Figure S1B) were counted in 3 independent experiments. Collagen degradation area of individual cells was determined from the immunofluorescent images of cells stained with anti-Col 1 - ¾ C antibody and fluorescently-labelled with phalloidin using Image J as described (Ferrari et al, 2019). Percentage of cells with nuclear localized β-catenin or emerin were determined from immunofluorescent images of cells stained with anti- β-catenin or anti-emerin antibodies, respectively, using Image J. Mean fluorescence density of active integrin β1 in each cell, F-actin area in phalloidin-stained cells and lamin A/C levels in individual cells were all measured with Image J. To image nuclear shape, SSCs embedded in collagen gels were fluorescently labelled with DAPI and phalloidin and Z-stack confocal images taken for 3D reconstruction (omitting cells lying within 50 um of the apical or basal face of 3D collagen gels) using an Imaris software system.

SiRNAs, Constructs and Gene Expression—Mouse Emerin siRNAs were purchased from Santa Cruz Technology and Millipore Sigma. For gene silencing, PepMute siRNA Transfection Reagent (SignaGen Laboratories) was used for transfection. Human mesenchymal stem cells obtained from Lonza were transfected using a human stem

cell Nucleofector kit (Lonza). Wild-type LmnA minigene, lamin A (R527P-mRFP), pBABE-puro-GFP-wt-lamin A and pMXs-β-catenin-S33Y were obtained from Addgene. A constitutively active β1 integrin mutant (G429N) was cloned into the pLentilox-IRS-GFP lentiviral vector as described (Tang et al., 2013). pBMN-Z retrovirus and DNKASHΔPPPL lentiviral constructs were obtained from Addgene, GFP-DNKASH vector was provided by Dr. P. Chavrier (Infante et al., 2018) and cloned into a pBMN-Z viral vector. SSCs were transduced with lentiviral or retroviral expression vectors and the expression of exogenous proteins confirmed by Western blot or immunofluorescence.

Immunoprecipitation and Immunoblotting—Neonatal skeletal homogenates or cell lysates were prepared using 2% SDS, RIPA buffer for Western blotting. For immunoprecipitation, cell lysates were prepared using a lysis buffer containing 50 mM Tris (pH 7.4), 150 mM NaCl, 1% Triton X-100 and 1 mM EDTA. The lysates were incubated with antibody and Dynabeads Protein G (Life Technologies). Following immunoprecipitation, immunocomplexes were analyzed by Western blotting. Integrated intensity of corresponding protein bands was quantified using Image J.

Histology—Neonatal or adult skeletal tissues were dissected and fixed overnight at 4°C in 4% paraformaldehyde in PBS. Adult bones were decalcified in 10% EDTA in PBS at 4°C. The skeletal specimens were embedded in OCT compound or paraffin, and sectioned (10 μm for cryostat sections and 5 μm for paraffin sections). Sections were stained with Hematoxylin/Eosin (H&E) according to standard procedures (Tang et al., 2013)(Tang et al., 2013)(Tang et al., 2013)(Tang et al., 2013)(Tang et al., 2013)(Tang et al., 2013).Femur osteoclasts were identified by staining for tartrate resistant acid phosphatase (TRAP) using a leukocyte acid phosphatase assay kit (Sigma-Aldrich). The number of TRAP-positive cells per millimeter of trabecular bone perimeter was quantified in the secondary spongiosa using ImageJ (Zhu et al., 2020).

Microcomputed Tomography—Femora from adult mice were fixed in 4% paraformaldehyde overnight at 4°C, and stored in 70% ethanol. Femurs were scanned in water at an 18 μm isotropic voxel resolution using Explore Locus SP (GE Healthcare Pre-Clinical Imaging, London, ON, Canada), and calibrated 3D images reconstructed. Bone morphometric variables were analyzed, including Bone Volume/Tissue Volume (BV/TV), Trabecular Number (Tb.N), Trabecular Separation (Tb.Sp) and Trabecular Thickness (Tb.Th) as described (Zhu et al., 2020).

***In Vivo* Assay of SSCs Bone Formation Capacity—**For *in vivo* osteogenic differentiation, collagen gels (2.16 mg/ml) were prepared without or with 2×10^6 seeded mouse SSCs per ml were seeded into collagen gels, allowed to gel, and then implanted subcutaneously into Nu/Nu mice. The specimens were dissected from the mouse recipients and analyzed 3 weeks later as described (Tang et al., 2013). Bone Volume/Tissue Volume (BV/TV) was measured with Image J.

Skeletal Analysis—Skulls collected at P2 were skinned, and fixed in 95% ethanol. Skull tissues were stained with Alizarin Red S and Alcian Blue as described (Tang et al., 2016).

Collagen Gel Contraction Assays—Collagen gel plug contraction assays were performed as described (Tang et al., 2013). Briefly, 1×10^6 SSCs per ml were embedded into 2.16 mg/ml rat tail-derived type I collagen gels (Tang et al., 2013) and cultured in 24-well plates for 48 hours. The collagen gels were manually detached from 24-well plates, and further cultured as floating constructs in 6-well plates for 4 hr. Images of the collagen gel plugs were acquired using a stereo microscope (Leica Microsystem), the diameters of the gel plugs measured and analyzed with Image J.

QUANTIFICATION AND STATISTICAL ANALYSIS

Statistical analysis was performed with Prism software (Graphpad Prism 8). The results are shown as mean±s.e.m. and p values determined using the Student's t-test or by analysis of variance (ANOVA). *: $p<0.05$, **: $p<0.01$. All statistical tests were two-sided. All experiments were repeated 3 times in independent determinations. Otherwise, the sample number (n) was shown in each figure legend.

Supplementary Material

Refer to Web version on PubMed Central for supplementary material.

Acknowledgements

Funding for this project was provided by the National Institutes of Health (SJW: CA071699, AR065524) and by the Breast Cancer Research Foundation (SJW). We thank Prof. Katherine Wilson (Johns Hopkins) for careful discussion.

References

Alisafaei F, Jokhun DS, Shivashankar GV, and Shenoy VB (2019). Regulation of nuclear architecture, mechanics, and nucleocytoplasmic shuttling of epigenetic factors by cell geometric constraints. Proc Natl Acad Sci U S A 116, 13200–13209. [PubMed: 31209017]

Baron R, and Kneissel M (2013). WNT signaling in bone homeostasis and disease: from human mutations to treatments. Nat Med 19, 179–192. [PubMed: 23389618]

Baryawno N, Przybylski D, Kowalczyk MS, Kfoury Y, Severe N, Gustafsson K, Kokkaliaris KD, Mercier F, Tabaka M, Hofree M, et al. (2019). A cellular taxonomy of the bone marrow stroma in homeostasis and leukemia. Cell 177, 1915–1932. [PubMed: 31130381]

Bermeo S, Vidal C, Zhou H, and Duque G (2015). Lamin A/C acts as an essential factor in mesenchymal stem cell differentiation through the regulation of the dynamics of the Wnt/beta-catenin pathway. J Cell Biochem 116, 2344–2353. [PubMed: 25846419]

Buxboim A, Swift J, Irianto J, Spinler KR, Dingal PC, Athirasala A, Kao YR, Cho S, Harada T, Shin JW, et al. (2014). Matrix elasticity regulates lamin-A,C phosphorylation and turnover with feedback to actomyosin. Curr Biol 24, 1909–1917. [PubMed: 25127216]

Chaudhuri O, Cooper-White J, Janmey PA, Mooney DJ, and Shenoy VB (2020). Effects of extracellular matrix viscoelasticity on cellular behaviour. Nature 584, 535–546. [PubMed: 32848221]

Chen J, and Long F (2013). beta-catenin promotes bone formation and suppresses bone resorption in postnatal growing mice. J Bone Miner Res 28, 1160–1169. [PubMed: 23188722]

Cho S, Vashisth M, Abbas A, Majkut S, Vogel K, Xia Y, Ivanovska IL, Irianto J, Tewari M, Zhu K, et al. (2019). Mechanosensing by the lamina protects against nuclear rupture, DNA damage, and cell-cycle arrest. Dev Cell 49, 920–935. [PubMed: 31105008]

Chun TH, Hotary KB, Sabeh F, Saltiel AR, Allen ED, and Weiss SJ (2006). A pericellular collagenase directs the 3-dimensional development of white adipose tissue. Cell 125, 577–591. [PubMed: 16678100]

Clevers H, and Nusse R (2012). Wnt/beta-catenin signaling and disease. Cell 149, 1192–1205. [PubMed: 22682243]

Csoka AB, English SB, Simkevich CP, Ginzinger DG, Butte AJ, Schatten GP, Rothman FG, and Sedivy JM (2004). Genome-scale expression profiling of Hutchinson-Gilford progeria syndrome reveals widespread transcriptional misregulation leading to mesodermal/mesenchymal defects and accelerated atherosclerosis. Aging Cell 3, 235–243. [PubMed: 15268757]

Day TF, Guo X, Garrett-Beal L, and Yang Y (2005). Wnt/beta-catenin signaling in mesenchymal progenitors controls osteoblast and chondrocyte differentiation during vertebrate skeletogenesis. Dev Cell 8, 739–750. [PubMed: 15866164]

Ehrbar M, Sala A, Lienemann P, Ranga A, Mosiewicz K, Bittermann A, Rizzi SC, Weber FE, and Lutolf MP (2011). Elucidating the role of matrix stiffness in 3D cell migration and remodeling. Biophys J 100, 284–293. [PubMed: 21244824]

Feinberg TY, Zheng H, Liu R, Wicha MS, Yu SM, and Weiss SJ (2018). Divergent matrix-remodeling strategies distinguish developmental from neoplastic mammary epithelial cell invasion programs. Dev Cell 47, 145–160. [PubMed: 30269950]

Ferrari R, Martin G, Tagit O, Guichard A, Cambi A, Voituriez R, Vassilopoulos S, and Chavrier P (2019). MT1-MMP directs force-producing proteolytic contacts that drive tumor cell invasion. Nat Commun 10, 4886. [PubMed: 31653854]

Fields GB (2019). The rebirth of matrix metalloproteinase inhibitors: Moving beyond the dogma. Cells 8, 984.

Guilluy C, Osborne LD, Van Landeghem L, Sharek L, Superfine R, Garcia-Mata R, and Burridge K (2014). Isolated nuclei adapt to force and reveal a mechanotransduction pathway in the nucleus. Nat Cell Biol 16, 376–381. [PubMed: 24609268]

Heo SJ, Driscoll TP, Thorpe SD, Nerurkar NL, Baker BM, Yang MT, Chen CS, Lee DA, and Mauck RL (2016). Differentiation alters stem cell nuclear architecture, mechanics, and mechano-sensitivity. Elife 5, e18207. [PubMed: 27901466]

Hernandez L, Roux KJ, Wong ES, Mounkes LC, Mutalif R, Navasankari R, Rai B, Cool S, Jeong JW, Wang H, et al. (2010). Functional coupling between the extracellular matrix and nuclear lamina by Wnt signaling in progeria. Dev Cell 19, 413–425. [PubMed: 20833363]

Ho CY, Jaalouk DE, Vartiainen MK, and Lammerding J (2013). Lamin A/C and emerin regulate MKL1-SRF activity by modulating actin dynamics. Nature 497, 507–511. [PubMed: 23644458]

Holmbeck K, Bianco P, Caterina J, Yamada S, Kromer M, Kuznetsov SA, Mankani M, Robey PG, Poole AR, Pidoux I, et al. (1999). MT1-MMP-deficient mice develop dwarfism, osteopenia, arthritis, and connective tissue disease due to inadequate collagen turnover. Cell 99, 81–92. [PubMed: 10520996]

Holt I, Ostlund C, Stewart CL, Man N, Worman HJ, and Morris GE (2003). Effect of pathogenic mis-sense mutations in lamin A on its interaction with emerin in vivo. J Cell Sci 116, 3027–3035. [PubMed: 12783988]

Infante E, Castagnino A, Ferrari R, Monteiro P, Aguera-Gonzalez S, Paul-Gilloteaux P, Domingues MJ, Maiuri P, Raab M, Shanahan CM, et al. (2018). LINC complex-Lis1 interplay controls MT1-MMP matrix digest-on-demand response for confined tumor cell migration. Nat Commun 9, 2443. [PubMed: 29934494]

Jones DL, and Wagers AJ (2008). No place like home: anatomy and function of the stem cell niche. Nat Rev Mol Cell Biol 9, 11–21. [PubMed: 18097443]

Kim Y, and Zheng Y (2013). Generation and characterization of a conditional deletion allele for Lmna in mice. Biochem Biophys Res Commun 440, 8–13. [PubMed: 23998933]

Kirby TJ, and Lammerding J (2018). Emerging views of the nucleus as a cellular mechanosensor. Nat Cell Biol 20, 373–381. [PubMed: 29467443]

Le HQ, Ghatak S, Yeung CY, Tellkamp F, Gunschmann C, Dieterich C, Yeroslaviz A, Habermann B, Pombo A, Niessen CM, et al. (2016). Mechanical regulation of transcription controls Polycomb-

mediated gene silencing during lineage commitment. Nat Cell Biol 18, 864–875. [PubMed: 27398909]

Lele TP, Dickinson RB, and Gundersen GG (2018). Mechanical principles of nuclear shaping and positioning. J Cell Biol 217, 3330–3342. [PubMed: 30194270]

Li W, Yeo LS, Vidal C, McCorquodale T, Herrmann M, Fatkin D, and Duque G (2011). Decreased bone formation and osteopenia in lamin a/c-deficient mice. PLoS One 6, e19313. [PubMed: 21547077]

Markiewicz E, Tilgner K, Barker N, van de Wetering M, Clevers H, Dorobek M, Hausmanowa-Petrusewicz I, Ramaekers FC, Broers JL, Blankesteijn WM, et al. (2006). The inner nuclear membrane protein emerin regulates beta-catenin activity by restricting its accumulation in the nucleus. EMBO J 25, 3275–3285. [PubMed: 16858403]

Matsushita Y, Nagata M, Kozloff KM, Welch JD, Mizuhashi K, Tokavanich N, Hallett SA, Link DC, Nagasawa T, Ono W, et al. (2020). A Wnt-mediated transformation of the bone marrow stromal cell identity orchestrates skeletal regeneration. Nat Commun 11, 332. [PubMed: 31949165]

Mirza AN, McKellar SA, Urman NM, Brown AS, Hollmig T, Aasi SZ, and Oro AE (2019). LAP2 proteins chaperone GLI1 movement between the lamina and chromatin to regulate transcription. Cell 176, 198–212 e115. [PubMed: 30503211]

Murphy MP, Koepke LS, Lopez MT, Tong X, Ambrosi TH, Gulati GS, Marecic O, Wang Y, Ransom RC, Hoover MY, et al. (2020). Articular cartilage regeneration by activated skeletal stem cells. Nat Med 26, 1583–1592. [PubMed: 32807933]

Neumann S, Schneider M, Daugherty RL, Gottardi CJ, Eming SA, Beijer A, Noegel AA, and Karakesisoglou I (2010). Nesprin-2 interacts with {alpha}-catenin and regulates Wnt signaling at the nuclear envelope. J Biol Chem 285, 34932–34938. [PubMed: 20801886]

Nikolova V, Leimena C, McMahon AC, Tan JC, Chandar S, Jogia D, Kesteven SH, Michalicek J, Otway R, Verheyen F, et al. (2004). Defects in nuclear structure and function promote dilated cardiomyopathy in lamin A/C-deficient mice. J Clin Invest 113, 357–369. [PubMed: 14755333]

Ono N, Balani DH, and Kronenberg HM (2019). Stem and progenitor cells in skeletal development. Curr Top Dev Biol 133, 1–24. [PubMed: 30902249]

Pan D, Estevez-Salmeron LD, Stroschein SL, Zhu X, He J, Zhou S, and Luo K (2005). The integral inner nuclear membrane protein MAN1 physically interacts with the R-Smad proteins to repress signaling by the transforming growth factor-{beta} superfamily of cytokines. J Biol Chem 280, 15992–16001. [PubMed: 15647271]

Pan JX, Xiong L, Zhao K, Zeng P, Wang B, Tang FL, Sun D, Guo HH, Yang X, Cui S, et al. (2018). YAP promotes osteogenesis and suppresses adipogenic differentiation by regulating beta-catenin signaling. Bone Res 6, 18. [PubMed: 29872550]

Paszek MJ, Zahir N, Johnson KR, Lakins JN, Rozenberg GI, Gefen A, Reinhart-King CA, Margulies SS, Dembo M, Boettiger D, et al. (2005). Tensional homeostasis and the malignant phenotype. Cancer Cell 8, 241–254. [PubMed: 16169468]

Rauch A, Haakonsson AK, Madsen JGS, Larsen M, Forss I, Madsen MR, Van Hauwaert EL, Wiwie C, Jespersen NZ, Tencerova M, et al. (2019). Osteogenesis depends on commissioning of a network of stem cell transcription factors that act as repressors of adipogenesis. Nat Genet 51, 716–727. [PubMed: 30833796]

Rauch A, and Mandrup S (2021). Transcriptional networks controlling stromal cell differentiation. Nat Rev Mol Cell Biol 22, 465–482. [PubMed: 33837369]

Serowoky MA, Arata CE, Crump JG, and Mariani FV (2020). Skeletal stem cells: insights into maintaining and regenerating the skeleton. Development 147, dev179325. [PubMed: 32161063]

Smith LR, Cho S, and Discher DE (2018). Stem cell differentiation is regulated by extracellular matrix mechanics. Physiology (Bethesda) 33, 16–25. [PubMed: 29212889]

Song L, Liu M, Ono N, Bringhurst FR, Kronenberg HM, and Guo J (2012). Loss of wnt/beta-catenin signaling causes cell fate shift of preosteoblasts from osteoblasts to adipocytes. J Bone Miner Res 27, 2344–2358. [PubMed: 22729939]

Stubenvoll A, Rice M, Wietelmann A, Wheeler M, and Braun T (2015). Attenuation of Wnt/beta-catenin activity reverses enhanced generation of cardiomyocytes and cardiac defects caused by the loss of emerin. Hum Mol Genet 24, 802–813. [PubMed: 25274778]

Sullivan T, Escalante-Alcalde D, Bhatt H, Anver M, Bhat N, Nagashima K, Stewart CL, and Burke B (1999). Loss of A-type lamin expression compromises nuclear envelope integrity leading to muscular dystrophy. J Cell Biol 147, 913–920. [PubMed: 10579712]

Swift J, Ivanovska IL, Buxboim A, Harada T, Dingal PC, Pinter J, Pajerowski JD, Spinler KR, Shin JW, Tewari M, et al. (2013). Nuclear lamin-A scales with tissue stiffness and enhances matrix-directed differentiation. Science 341, 1240104. [PubMed: 23990565]

Tang CY, Wu M, Zhao D, Edwards D, McVicar A, Luo Y, Zhu G, Wang Y, Zhou HD, Chen W, et al. (2021). Runx1 is a central regulator of osteogenesis for bone homeostasis by orchestrating BMP and WNT signaling pathways. PLoS Genet 17, e1009233. [PubMed: 33476325]

Tang Y, Feinberg T, Keller ET, Li XY, and Weiss SJ (2016). Snail/Slug binding interactions with YAP/TAZ control skeletal stem cell self-renewal and differentiation. Nat Cell Biol 18, 917–929. [PubMed: 27479603]

Tang Y, Rowe RG, Botvinick EL, Kurup A, Putnam AJ, Seiki M, Weaver VM, Keller ET, Goldstein S, Dai J, et al. (2013). MT1-MMP-dependent control of skeletal stem cell commitment via a beta1-integrin/YAP/TAZ signaling axis. Dev Cell 25, 402–416. [PubMed: 23685250]

Uzer G, Bas G, Sen B, Xie Z, Birks S, Olcum M, McGrath C, Styner M, and Rubin J (2018). Sun-mediated mechanical LINC between nucleus and cytoskeleton regulates betacatenin nuclear access. J Biomech 74, 32–40. [PubMed: 29691054]

Vaughan A, Alvarez-Reyes M, Bridger JM, Broers JL, Ramaekers FC, Wehnert M, Morris GE, Whitfield WGF, and Hutchison CJ (2001). Both emerin and lamin C depend on lamin A for localization at the nuclear envelope. J Cell Sci 114, 2577–2590. [PubMed: 11683386]

Walma DAC, and Yamada KM (2020). The extracellular matrix in development. Development 147, dev175596. [PubMed: 32467294]

Wells JM, Gaggar A, and Blalock JE (2015). MMP generated matrikines. Matrix Biol 44–46, 122–129.

Yook JI, Li XY, Ota I, Hu C, Kim HS, Kim NH, Cha SY, Ryu JK, Choi YJ, Kim J, et al. (2006). A Wnt-Axin2-GSK3beta cascade regulates Snail1 activity in breast cancer cells. Nat Cell Biol 8, 1398–1406. [PubMed: 17072303]

Zhang Q, Narayanan V, Mui KL, O'Bryan CS, Anderson RH, Kc B, Cabe JI, Denis KB, Antoku S, Roux KJ, et al. (2019). Mechanical stabilization of the glandular acinus by linker of nucleoskeleton and cytoskeleton complex. Curr Biol 29, 2826–2839. [PubMed: 31402305]

Zhao H, Feng J, Ho TV, Grimes W, Urata M, and Chai Y (2015). The suture provides a niche for mesenchymal stem cells of craniofacial bones. Nat Cell Biol 17, 386–396. [PubMed: 25799059]

Zhu L, Tang Y, Li XY, Keller ET, Yang J, Cho JS, Feinberg TY, and Weiss SJ (2020). Osteoclast-mediated bone resorption is controlled by a compensatory network of secreted and membrane-tethered metalloproteinases. Sci Transl Med 12, eaaw6143. [PubMed: 32024800]

Highlights

- ECM remodeling regulates Wnt signaling to control skeletal stem cell (SSC) fate
- MMP14-driven remodeling modulates lamin A/C via LINC-dependent mechanotransduction
- A lamin A/C-emerin node regulates nuclear β-catenin-mediated Wnt signaling
- SSC lineage is regulated by an MMP14-nuclear lamin A/C-emerin-β-catenin network

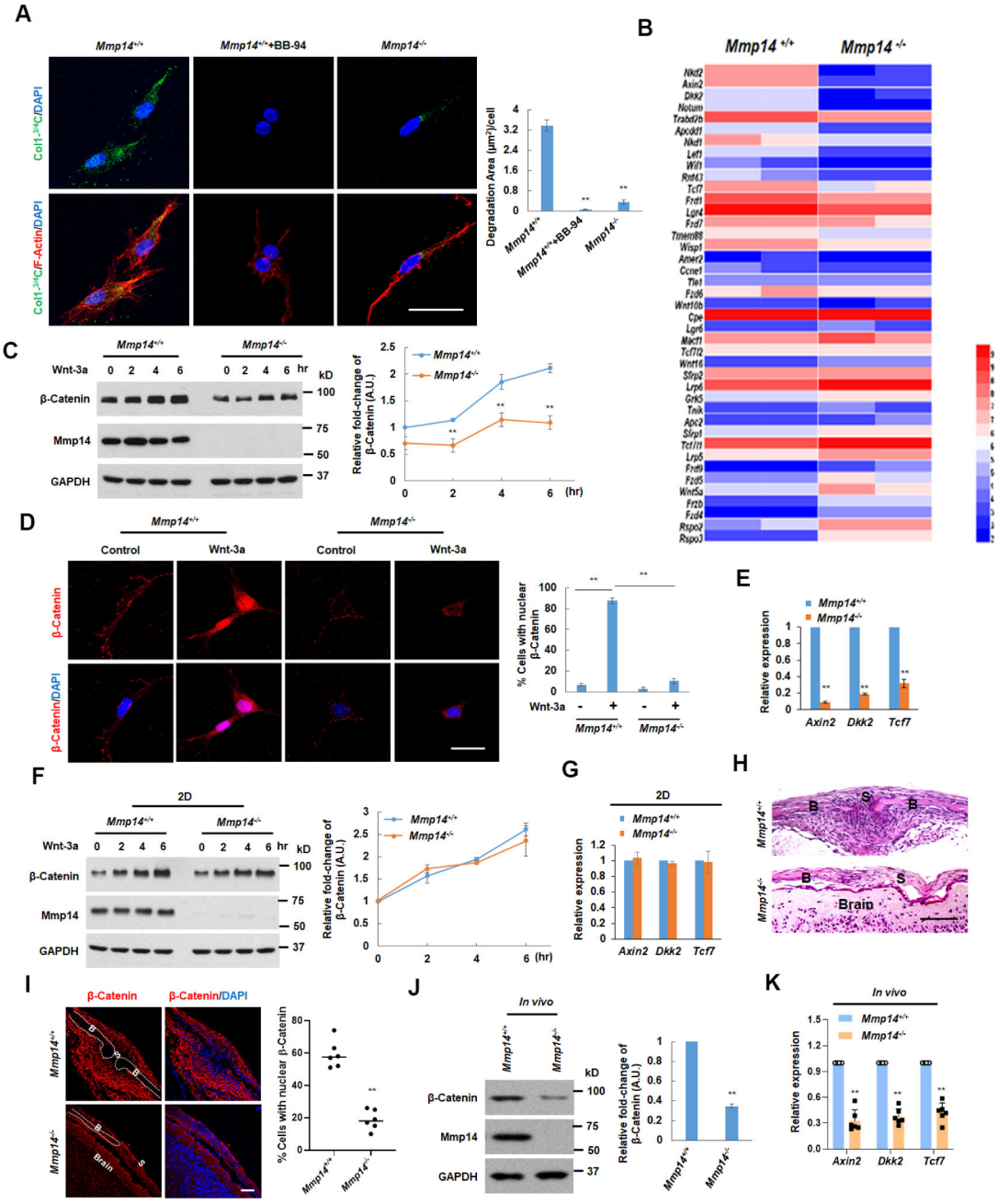

Figure 1.

ECM remodeling regulates Wnt signaling.

A. Immunofluorescence staining of cleaved collagen neoepitope (Col1-$^{3/4}$C antibody, green), F-actin (red) and DAPI (blue) in SSCs isolated from *Mmp14*$^{+/+}$ or *Mmp14*$^{-/-}$ mice cultured in 3D collagen gels and incubated without or with BB-94 (5 μM) for 48 hr as assessed by confocal imaging. Right panel: quantitation of the cleaved collagen. Scale bar: 8 μm. Mean±s.e.m. (n=3) by ANOVA, **p<0.01.

B. Heat map of Wnt signaling pathway-associated transcripts detected in SSCs isolated from *Mmp14*$^{+/+}$ or *Mmp14*$^{-/-}$ mice, and cultured in 3D collagen gels for 48 hr. Results are from 2 representative exps.

C. Western blot of active (non-phosphorylated) β-catenin in SSCs isolated from *Mmp14*$^{+/+}$ or *Mmp14*$^{-/-}$ mice and cultured in 3D collagen gels without or with recombinant Wnt-3a (100 ng/ml) for the indicated times. Right panel: Quantitation of β-catenin levels (β-catenin in *Mmp14*$^{+/+}$ cells at time 0 set to a value of 1). Mean±s.e.m. (n=3) by Student's t test, **p<0.01.

D. Z-stack confocal images of active β-catenin in SSCs from (C) treated without or with Wnt-3a (100 ng/ml) for 4 hr. Scale bar: 10 μm. Right panel: quantitation of nuclear β-catenin^{+} cells. Mean±s.e.m. (n=3 with 50 cells randomly scored/exp) by ANOVA, **p<0.01.

E. RT-PCR of Wnt signaling target genes in SSCs from (C) cultured with Wnt-3a (100 ng/ml) for 4 hr. Mean±s.e.m. (n=3) by Student's t test, **p<0.01.

F. Western blot of active β-catenin in SSCs isolated from *Mmp14*$^{+/+}$ or *Mmp14*$^{-/-}$ mice and cultured in 2D without or with Wnt-3a (100 ng/ml) for indicated times. Right panel: quantitation of β-catenin levels (β-catenin in *Mmp14*$^{+/+}$ cells at time 0 set as 1). Mean±s.e.m. (n=3) by Student's t test, **p<0.01.

G. RT-PCR of Wnt-targeted genes in SSCs from (F) cultured with Wnt-3a (100 ng/ml) for 4 hr. Mean±s.e.m. (n=3) by Student's t test, **p<0.01.

H. Histology of parietal bone from P0 *Mmp14*$^{+/+}$ or *Mmp14*$^{-/-}$ mice. Scale bar: 100 μm. B: bone, S: Suture. Results representative of 3 exps performed.

I. Z-stack confocal images of active β-catenin in parietal bone from P0 *Mmp14*$^{+/+}$ or *Mmp14*$^{-/-}$. Scale bar: 25 μm. B: bone, S: Suture. Right panel: quantitation of nuclear β-catenin-positive cells. (n=6; 100 cells randomly imaged in each suture) by Student's t test, **p<0.01.

J. Western blot of active β-catenin in calvaria lysates from P0 *Mmp14*$^{+/+}$ or *Mmp14*$^{-/-}$ mice. Right panel: quantitation of β-catenin levels. Mean±s.e.m. (n=3) by Student's t test, **p<0.01.

K. RT-PCR of Wnt signaling target genes in calvarial extracts from P0 *Mmp14*$^{+/+}$ or *Mmp14*$^{-/-}$ mice. Mean±s.e.m. (n=6) as assessed by Student's t test, ** p<0.01.

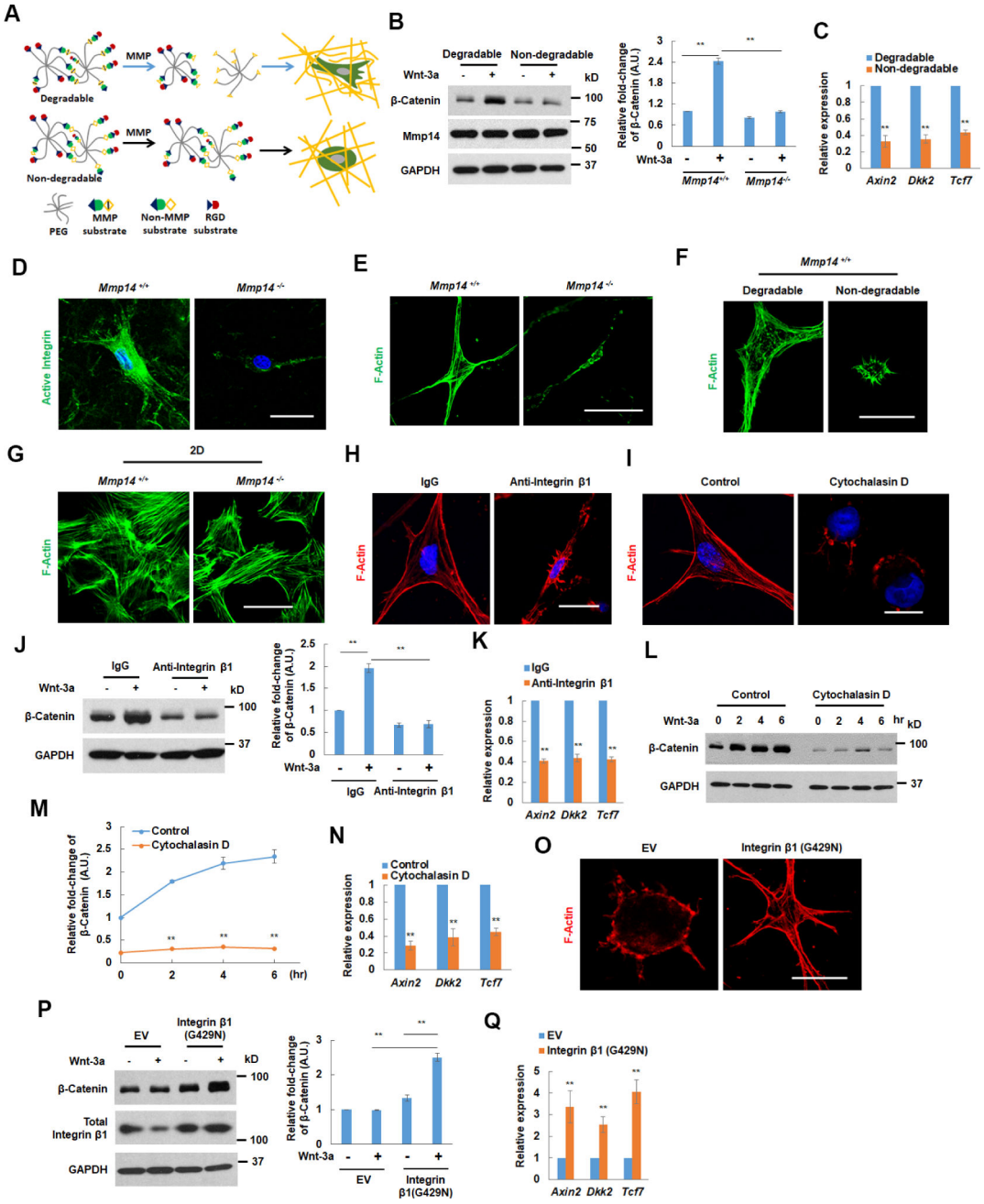

Figure 2.

ECM remodeling regulates Wnt signaling by triggering cytoskeletal reorganization.

A. Schematic of PEG-based hydrogel harboring MMP -sensitive or -insensitive peptides cross-linked to a PEG backbone decorated with cell-adhesive RGD.

B. Western blot of active β-catenin in *Mmp14*$^{+/+}$ SSCs cultured in degradable or non-degradable PEG-based hydrogels with or without Wnt-3a (100 ng/ml) for 4 hr. Right panel: Quantitation of β-catenin levels (cells cultured in degradable gels without Wnt-3a are set to a value of 1). Mean±s.e.m. (n=3) by ANOVA, **p<0.01.

C. RT-PCR of Wnt target genes in SSCs from (B) cultured with Wnt-3a (100 ng/ml) for 4 hr. Mean±s.e.m. (n=3) by Student's t test, ** p<0.01.

D. Z-stack confocal images of active integrin β1 in SSCs isolated from *Mmp14*$^{+/+}$ or *Mmp14*$^{-/-}$ mice cultured in 3D collagen gels for 4 hr. Scale bar: 5 μm. Results representative of 3 exps performed.

E. Z-stack confocal images of phalloidin-stained SSCs isolated from *Mmp14*$^{+/+}$ or *Mmp14*$^{-/-}$ mice and cultured in 3D collagen gel for 48 hr. Scale bar: 10 μm. Results representative of 3 exps performed.

F. Z-stack confocal images of phalloidin-stained SSCs isolated from *Mmp14*$^{+/+}$ or *Mmp14*$^{-/-}$ mice and cultured in 3D PEG hydrogels (MMP- degradable or non-degradable) for 7 d. Scale bar: 10 μm. Results representative of 3 exps performed.

G. Z-stack confocal images of phalloidin-stained SSCs isolated from *Mmp14*$^{+/+}$ or *Mmp14*$^{-/-}$ mice and cultured atop 2D glass surfaces for 48 hr. Scale bar: 10 μm. Results representative of 3 exps performed.

H. Z-stack confocal images of phalloidin-stained *Mmp14*$^{+/+}$ SSCs cultured in 3D collagen gels with control IgG or anti-integrin β1 antibody (0.5 μg/ml) for 48 hr. Results representative of 3 exps performed. Scale bar: 5 μm.

I. Z-stack confocal images of phalloidin-stained *Mmp14*$^{+/+}$ SSCs cultured in 3D collagen gel and treated without (control) or with cytochalasin D (1 μM) for 36 hr. Results representative of 3 exps performed. Scale bar: 5 μm.

J. Western blot of active β-catenin in SSCs cultured in 3D collagen gels with control IgG or an anti-integrin-β1 antibody (0.5 μg/ml) for 24 hr and then treated without or with Wnt-3a (100 ng/ml) for 4 hr. Right panel: Quantitation of β-catenin levels (cells treated with IgG in the absence of Wnt-3a are set to a value of 1). Mean±s.e.m. (n=3) as by ANOVA, **p<0.01.

K. RT-PCR of Wnt target genes in SSCs from (J) cultured with Wnt-3a (100 ng/ml) for 4 hr. Mean±s.e.m. (n=3) by Student's t test, ** p<0.01.

L. Western blot of active β-catenin in *Mmp14*$^{+/+}$ SSCs cultured in 3D collagen gels with cytochalasin D (1 μM) for 36 hr and treated without or with Wnt-3a (100 ng/ml) for the indicated times. Results representative of 3 exps performed.

M. Quantitation of β-catenin levels for (L) with control group at time 0 set as 1. Mean±s.e.m. (n=3) by Student's t test, **p<0.01.

N. RT-PCR of Wnt signaling target genes in SSCs from (L) cultured with Wnt-3a (100 ng/ml) for 4 hr. Mean±s.e.m. (n=3) by Student's t test, ** p<0.01.

O. Z-stack confocal images of phalloidin-stained SSCs isolated from *Mmp14*$^{-/-}$ mice, transduced with a control lentiviral vector (EV) or a vector expressing an activated integrin-β1 mutant (G429N) and cultured in 3D collagen gels for 48 hr. Scale bar: 10 μm. Results representative of 3 exps performed.

P. Western blot of active β-catenin in SSCs from (O) treated without or with Wnt-3a (100 ng/ml) for 4 hr. Right panel: Quantitation of β-catenin levels (EV group cultured without Wnt-3a treatment set to a value of 1). Mean±s.e.m. (n=3) by ANOVA, **p<0.01.

Q. RT-PCR of Wnt target genes in SSCs from (O) cultured with Wnt-3a (100 ng/ml) for 4 hr. Mean±s.e.m. (n=3) by Student's t test, ** p<0.01.

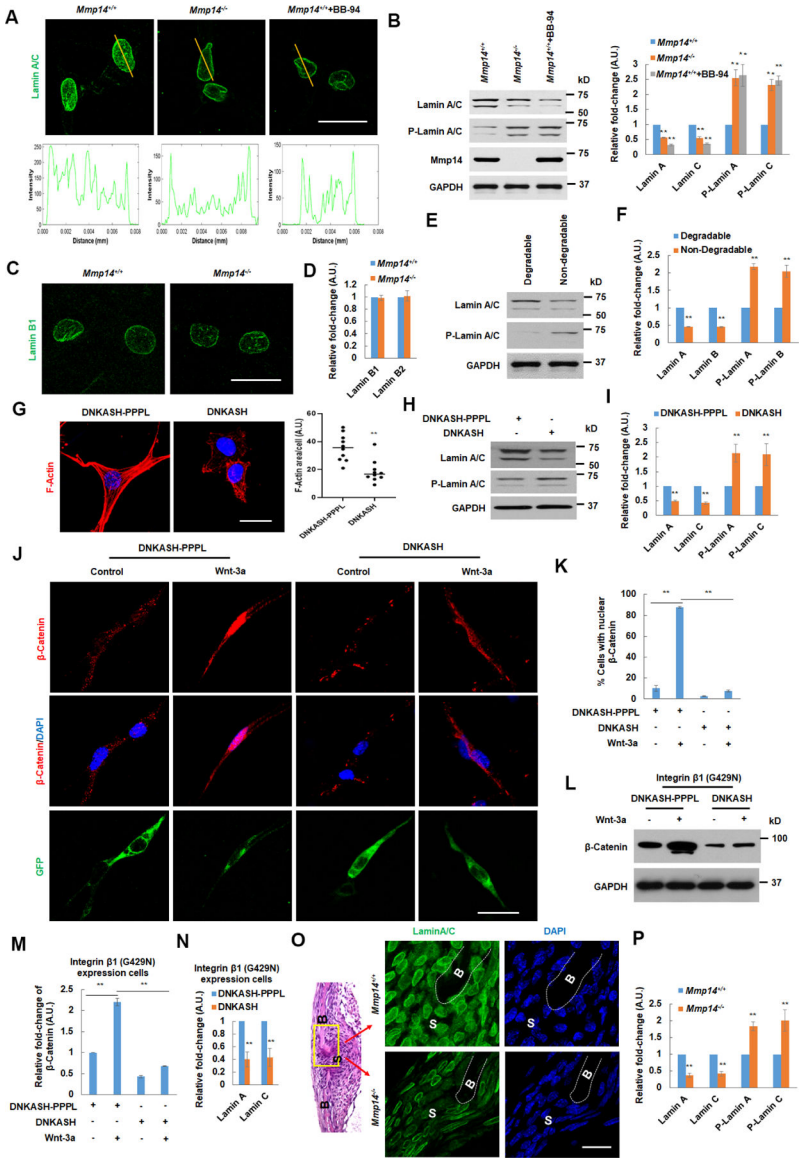

Figure 3.

LINC complexes couple nucleo- and cyto- skeletal organization with ECM remodeling to regulate Wnt signaling.

A. Z-stack confocal imaging of lamin A/C in SSCs isolated from *Mmp14*$^{+/+}$ or *Mmp14*$^{-/-}$ mice, cultured in 3D collagen gels and treated without or with BB-94 (5 μM) for 48 hr. Lower panel: Normalized fluorescence intensity profiles of lamin A/C along the yellow line crossing nuclei are shown. Scale bar: 10 μm. Results representative of 3 exps performed.

B. Western blot of lamin A/C and phosphorylated lamin A/C (P-Lamin A/C) in cells from (A). Right panel: Quantitation of protein levels. Mean±s.e.m. (n=3) by ANOVA, **p<0.01.

C. Z-stack confocal imaging of lamin B1 in SSCs isolated from *Mmp14*$^{+/+}$ or *Mmp14*$^{-/-}$ mice and cultured in 3D collagen gels for 48 hr. Scale bar: 10 μm. Results representative of 3 exps performed.

D. Western blot quantitation of lamin B1 and B2 expression in SSCs isolated from *Mmp14*$^{+/+}$ or *Mmp14*$^{-/-}$ mice and cultured in 3D collagen gels for 48 hr. Mean±s.e.m. (n=3) by Student's t test, **p<0.01.

E. Western blot of lamin A/C and P-lamin A/C in *Mmp14*$^{+/+}$ SSCs cultured in degradable or non-degradable PEG-based hydrogels for 7 d. Results representative of 3 exps performed.

F. Quantitation of lamin A/C and P-lamin A/C in cells from (E). Mean±s.e.m. (n=3) by Student's t test, **p<0.01.

G. Z-stack confocal imaging of phalloidin-stained SSCs isolated from *Mmp14*$^{+/+}$ mice and transduced with retroviral expression vectors encoding DNKASH-PPPL or a dominant-negative KASH (DNKASH) and cultured in 3D collagen gels for 48 hr. Scale bar: 10 μm. Right panel: Quantitation of F-actin in 10 randomly selected cells analyzed from each of 3 independent exps, ** p<0.01.

H. Western blot of lamin A/C and P-lamin A/C in SSCs from (G). Results representative of 3 exps performed.

I. Quantitation of lamin A/C and phosphorylated lamin A/C (P-Lamin A/C) expression in cells from (H). Mean±s.e.m. (n=3) by Student's t test, **p<0.01.

J. Z-stack confocal imaging of active β-catenin in SSCs from (G) treated with or without Wnt-3a (100 ng/ml) for 4hr. Scale bar: 10 μm. Results representative of 3 exps performed.

K. Quantitation of nuclear β-catenin positive cells from (J). Mean±s.e.m. (n=3 using 50 randomly scored cells/exp) by ANOVA, **p<0.01.

L. Western blot of active β-catenin in SSCs expressing a constitutively active β1 integrin mutant transduced with retroviral DNKASH-PPPL or DNKASH and cultured in 3D collagen gels for 48 hr. Cells were treated without or with Wnt-3a (100 ng/ml) for 4 hr. Results representative of 3 exps performed.

M. Quantitation of β-catenin levels for (L) with the DNKASH-PPPL group cultured without Wnt-3a set to a value of 1. Mean±s.e.m. (n=3) by ANOVA, **p<0.01.

N. Western blot quantitation of lamin A/C expression in SSCs expressing an active β1 integrin mutant were transduced with DNKASH-PPPL or DNKASH retroviral expression vectors and cultured in 3D collagen gels for 48 hr. Mean±s.e.m. (n=3) by Student's t test, **p<0.01.

O. Z-stack confocal imaging of lamin A/C in parietal bone from P0 *Mmp14*$^{+/+}$ or *Mmp14*$^{-/-}$ mice. Scale bar: 15 μm). B: Bone, S: Suture. Results representative of 3 exps performed.

P. Western blot quantitation of lamin A/C in protein lysates of calvaria recovered from P0 *Mmp14*$^{+/+}$ or *Mmp14*$^{-/-}$ mice. Mean±s.e.m. (n=3) by Student's t test, **p<0.01.

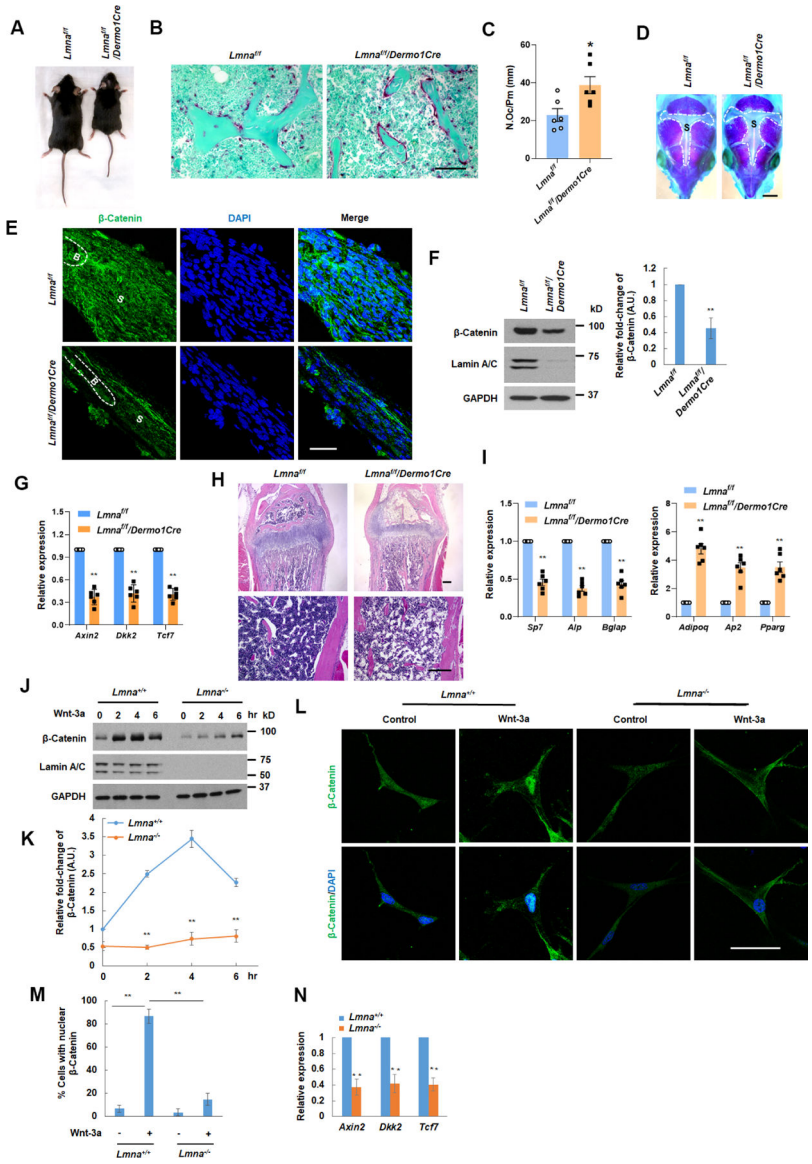

Figure 4.

Lamin A/C regulates Wnt signaling to control SSC differentiation.

A. A 3-month-old *Lmna*$^{f/f}$/*Dermo1-Cre* mouse and its control littermate (*Lmna*$^{f/f}$).

B. Osteoclast-specific TRAP/Fast Green staining of femurs from a 3 month-old *Lmna*$^{f/f}$/*Dermo1-Cre* mouse and control littermate (*Lmna*$^{f/f}$). Scale bar: 100 μm. Results representative of 3 exps performed.

C. Quantitation of osteoclast numbers in sections from images shown in (B). Number of Osteoclasts/Perimeter (mm) (N.Oc/Pm (mm)) are shown. Mean±s.e.m. (n=6) as by Student's t test, * $p<0.05$.

D. Alizarin Red/Alcian Blue staining of skulls isolated from P2 *Lmna*$^{f/f}$ and *Lmna*$^{f/f}$ / *Dermo1Cre* mice. Scale bar: 2 mm. White dotted line indicates the suture area: S. Results representative of 3 exps performed.

E. Z-stack confocal imaging of active β-catenin in parietal bone from P2 *Lmna*$^{f/f}$ and *Lmna*$^{f/f}$*/Dermo1Cre* mice. Scale bar: 50 μm. (B: Bone, S: Suture). Results representative of 3 exps performed.

F. Western blot and quantitation of active β-catenin in lysates recovered from calvaria of P2 *Lmna*$^{f/f}$ and *Lmna*$^{f/f}$*/Dermo1Cre* mice. Mean±s.e.m. (n=3) by Student's t test, **p<0.01.

G. Relative expression of Wnt target genes in calvarial extracts from P2 *Lmna*$^{f/f}$ and *Lmna*$^{f/f}$*/Dermo1Cre* mice. Mean±s.e.m. (n=6) by Student's t test, ** p<0.01.

H. Histology of tibia from 3-month old *Lmna*$^{f/f}$ and *Lmna*$^{f/f}$ */Dermo1Cre* conditional knockout mice. Lower panels show high magnification images highlighting adipogenesis. Scale bar: 100 μm. Results representative of 3 exps performed.

I. Relative mRNA expression of adipogenic and osteogenic markers in bone marrow RNA isolated from 3 month-old *Lmna*$^{f/f}$ and *Lmna*$^{f/f}$*/Dermo1Cre* mice. Mean±s.e.m. (n=6) by Student's t test, ** p<0.01.

J. Western blot of active β-catenin in SSCs from *Lmna*$^{+/+}$ or *Lmna*$^{-/-}$ mice incubated alone or with Wnt-3a (100 ng/ml) for indicated times. Results are representative of 3 exps performed.

K. Quantitation of β-catenin levels for (J) with β-catenin in *Lmna*$^{+/+}$ cells at time 0 set at 1. Mean±s.e.m. (n=3) by Student's t test, **p<0.01.

L. Z-stack confocal imaging of active β-catenin in SSCs isolated from *Lmna*$^{+/+}$ or *Lmna*$^{-/-}$ mice and cultured in 3D collagen gels treated with Wnt-3a (100 ng/ml) for 4 hr. Scale bar: 10 μm. Results are representative of 3 exps performed.

M. Quantitation of nuclear β-catenin^{+} cells from (L). Mean±s.e.m. (n=3 with 50 randomly selected cells scored/experiment) by ANOVA, **p<0.01.

N. Relative mRNA expression of Wnt target genes in SSCs from (L) treated with Wnt-3a (100 ng/ml) for 4 hr. Mean±s.e.m. (n=3) by Student's t test, ** p<0.01.

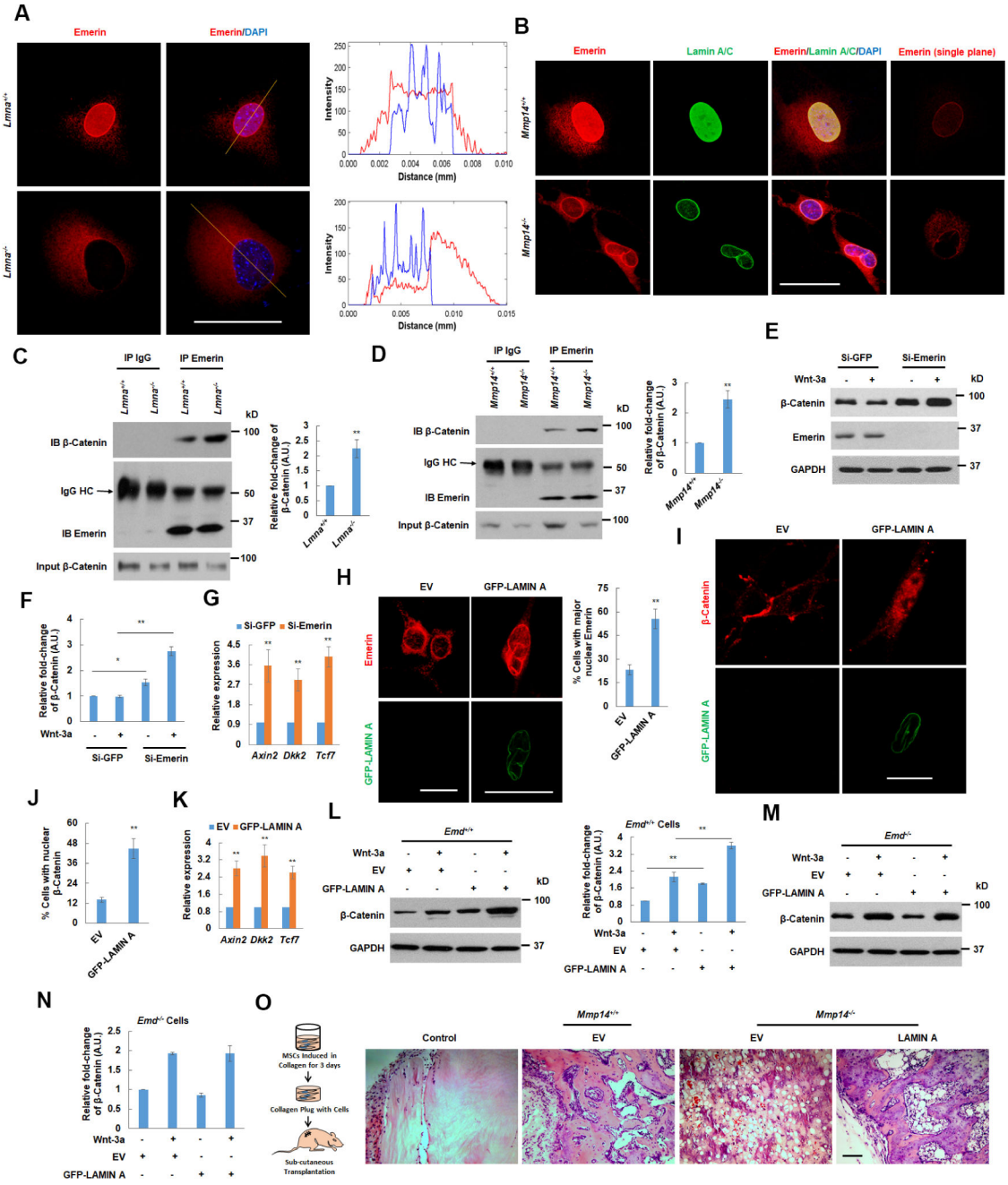

Figure 5.

Nucleoskeletal control of emerin/β-catenin complexes regulates Wnt signaling and SSC differentiation.

A. Z-stack confocal imaging of emerin in SSCs isolated from *Lmna*$^{+/+}$ or *Lmna*$^{-/-}$ mice and cultured atop 2D atop glass surfaces for 48 hr. Right panels: Normalized fluorescence intensity profiles of emerin (red) and DAPI (blue) along the yellow line crossing cells are shown. Scale bar: 10 μm. Results representative of 3 exps performed.

B. Z-stack confocal images of emerin and lamin A/C in SSCs isolated from *Mmp14*$^{+/+}$ or *Mmp14*$^{-/-}$ mice and cultured in 3D collagen for 48 hr are shown for the first 3 sets of

panels. Single confocal plane images of emerin are shown in the far right panels. Scale bar: 10 μm. Results representative of 3 exps performed.

C. Immunoprecipitation of emerin/β-catenin complexes in SSCs isolated from *Lmna*$^{+/+}$ or *Lmna*$^{-/-}$ mice and cultured in 3D collagen gels for 48 hr. Right panel: Quantitation of emerin/β-catenin complexes. Mean±s.e.m. (n=3) by Student's t test, **p<0.01.

D. Immunoprecipitation of emerin/β-catenin complexes in SSCs isolated from *Mmp14*$^{+/+}$ or *Mmp14*$^{-/-}$ mice and cultured in 3D collagen gels for 48 hr. Right panel: Quantitation of emerin/β-catenin complexes. Mean±s.e.m. (n=3) by Student's t test, **p<0.01.

E. Western blot of active β-catenin in SSCs transfected with control (GFP) or emerin siRNAs and cultured in in 3D collagen gels without or with Wnt-3a (100 ng/ml) for 4 hr. Results representative of 3 exps performed.

F. Quantitation of β-catenin levels for (E) with si-GFP group cultured without Wnt-3a treatment set at 1. Mean±s.e.m. (n=3) by ANOVA, *p<0.05, **p<0.01.

G. Relative mRNA expression of Wnt target genes in SSCs transfected with control (GFP) or emerin siRNAs and cultured in 3D collagen gels without or with Wnt-3a (100 ng/ml) for 4 hr. Mean±s.e.m. (n=3) by Student's t test, ** p<0.01.

H. Z-stack confocal imaging of emerin in SSCs isolated from *Mmp14*$^{-/-}$ mice and transduced with an empty (EV) or GFP-LMNA expression vector and cultured in 3D collagen gels for 48 hr. Scale bar: 10 μm. Right panel: Quantitation of percent cells with distinct nuclear emerin staining. Mean±s.e.m. (n=3 with 30 randomly scored cells counted/exp) by Student's t test, ** p<0.01.

I. Z-stack confocal imaging of active β-catenin in SSCs from (H) treated with 100 ng/ml Wnt-3a for 4 hr. Scale bar: 10 μm. Results representative of 3 exps performed.

J. Quantitation of the percent cells with nuclear-stained β-catenin for (I). Mean±s.e.m. (n=3 with 50 randomly scored cells counted/exp) by Student's t test, ** p<0.01.

K. Relative mRNA expression of Wnt target genes in SSCs from (I). Mean±s.e.m. (n=3) by Student's t test, ** p<0.01.

L. Western blot of active β-catenin in SSCs isolated from *Emd*$^{+/+}$ mice, transduced with an empty (EV) or GFP-LMNA expression vector, cultured in 3D collagen gels for 48 hr, and treated with 100 ng/ml Wnt-3a for 4 hr. Scale bar: 10 μm. Right panel: Quantitation of β-catenin levels with the EV group cultured without Wnt-3a treatment set at 1. Mean±s.e.m. (n=3) by ANOVA, **p<0.01.

M. Western blot of active β-catenin in SSCs isolated from *Emd*$^{-/-}$ mice, transduced with an empty (EV) or GFP-LMNA expression vector, cultured in 3D collagen gels for 48 hr and treated with 100 ng/ml Wnt-3a for 4 hr. Scale bar: 10 μm.

N. Quantitation of β-catenin levels in (M) with the EV group cultured without Wnt-3a set at 1. Mean±s.e.m. (n=3) by ANOVA, **p<0.01.

O. Left panel: Schematic representation of the experimental design. Right panel: *Mmp14*$^{+/+}$ or *Mmp14*$^{-/-}$ SSCs were transduced with an empty (EV) or a GFP-LMNA expression vector, embedded in collagen gels, and implanted subcutaneously into nude mice. Control: collagen gel alone implanted into the nude mice. Three weeks later, implants were harvested, fixed and H&E-stained. Scale bar: 100 μm. Results representative of n=6 exps.

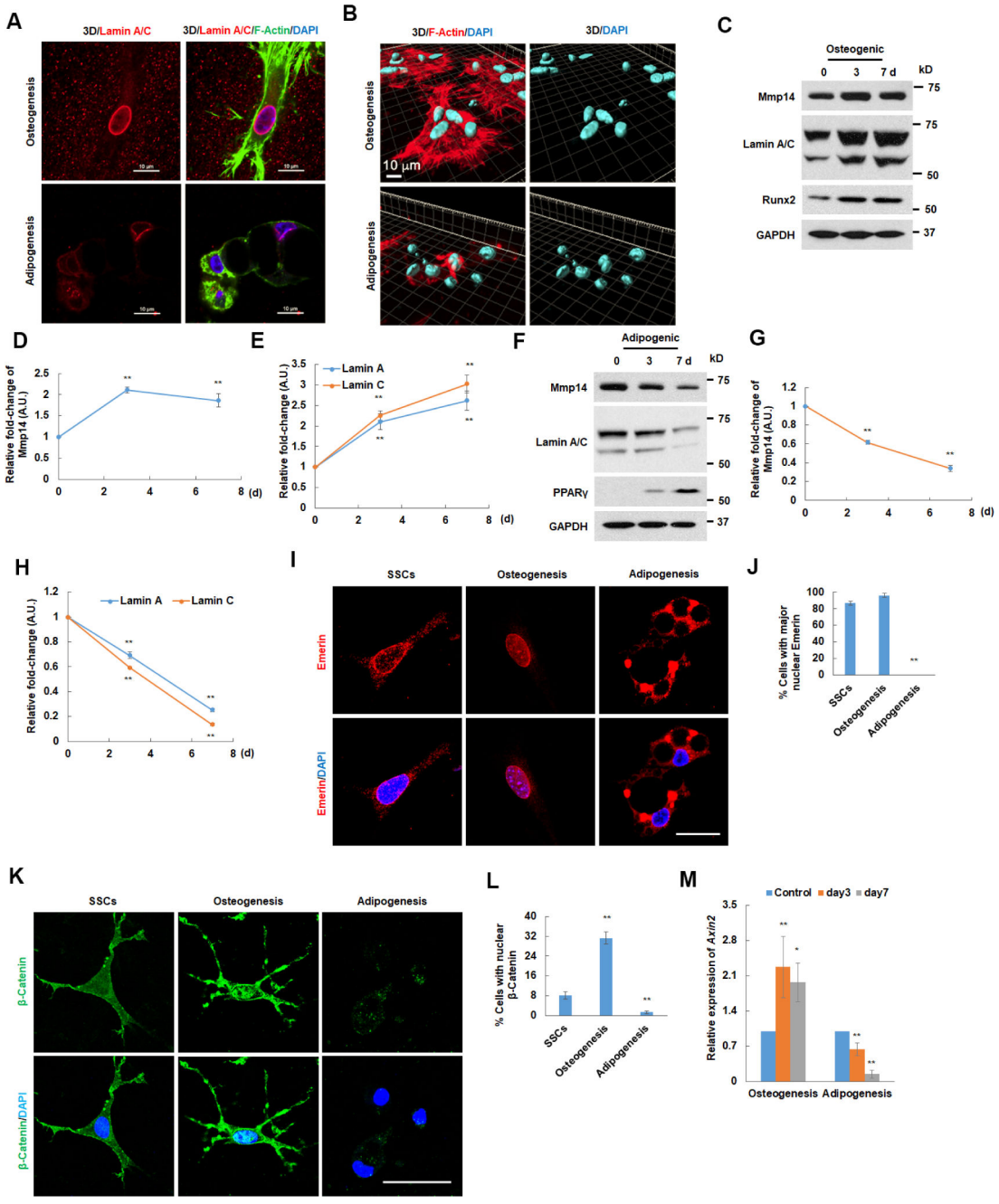

Figure 6.

Modulating Mmp14 activity, lamin A/C levels, emerin localization and Wnt signaling during osteogenic versus adipogenic commitment.

A. Z-stack confocal imaging of lamin A/C and F-actin in SSCs cultured in 3D collagen under osteogenic or adipogenic conditions for 7 d. Scale bar: 10 μm. Results representative of 3 exps performed.

B. Z-stack confocal imaging of phalloidin- and DAPI- stained SSCs from (A) in tandem with nuclear shape changes as shown in 3D reconstructions assembled by Imaris software. Scale bar: 10 μm. Results representative of 3 exps performed.

C. Western blot of Mmp14 and lamin A/C in SSCs cultured in 3D collagen with osteogenic induction for the indicated times. Results representative of 3 exps performed.
D. Quantitation of Mmp14 levels for (C) with time 0 values set at 1. Mean±s.e.m. (n=3) by ANOVA, **p<0.01.
E. Quantitation of lamin A/C levels for (C) with time 0 set to a value of 1. Mean±s.e.m. (n=3) by ANOVA, **p<0.01.
F. Western blot of Mmp14 and lamin A/C in SSCs cultured in 3D collagen with adipogenic induction for the indicated times. Results representative of 3 exps performed.
G. Quantitation of Mmp14 levels for (F) with time 0 set to a value 1. Mean±s.e.m. (n=3) by ANOVA, **p<0.01.
H. Quantitation of lamin A/C levels for (F) with time 0 set to a value of 1. Mean±s.e.m. (n=3) by ANOVA, **p<0.01.
I. Z-stack confocal images of emerin in SSCs cultured in 3D collagen under osteogenic or adipogenic conditions for 7 d. Scale bar: 7.5 μm. Results representative of 3 exps performed.
J. Quantitation of the percent cells with distinct nuclear-stained emerin for (I). Mean±s.e.m. (n=3 with 30 randomly scored cells scored/exp) by ANOVA, ** p<0.01.
K. Z-stack confocal images of active β-catenin in SSCs cultured in 3D collagen under osteogenic or adipogenic conditions for 7 d. Scale bar: 10 μm. Results representative of 3 exps performed.
L. Quantitation of the percent cells with nuclear-stained β-catenin in (K). Mean±s.e.m. (n=3 with 50 randomly scored cells scored/exp) by ANOVA, ** p<0.01.
M. *Axin2* expression in SSCs cultured in 3D collagen under osteogenic or adipogenic conditions for the indicated times. Mean±s.e.m. (n=3) by Student's t test, * p<0.05, ** p<0.01.

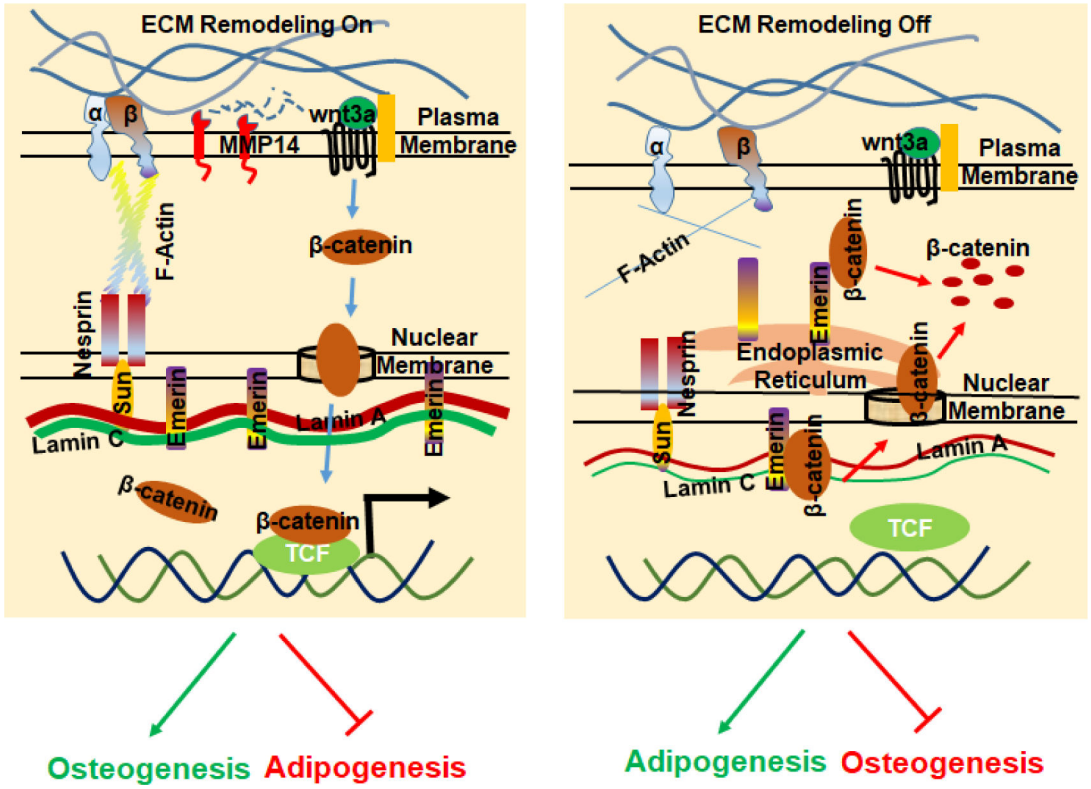

Figure 7.

Schematic model.

Mmp14-dependent ECM remodeling by SSCs triggers coordinated cell spreading and shape changes that lead to integrin activation and the induction of an F-actin/LINC/lamin A/C cascade that localizes emerin to the nuclear envelope, creating conditions permissive for nuclear β-catenin trafficking and the Wnt signaling programs necessary for osteogenic commitment. Alternatively, when adipogenic signals repress (or fail to trigger) Mmp14 activity, ECM remodeling is downregulated, thereby blunting the integrin signaling cascade and F-actin/LINC/lamin A/C mechanotransduction. As lamin A/C levels fall, emerin diffuses from the nuclear envelope into the ER where it serves as a β-catenin sink, thereby inhibiting Wnt signaling to allow adipogenesis to proceed.

KEY RESOURCE TABLE

REAGENT or RESOURCE	SOURCE	IDENTIFIER
Antibodies		
Alexa Fluor® 488 anti-mouse/rat CD29 Antibody	BioLegend	102212; RRID: AB_492829
APC anti-mouse Ly-6A/E (Sca-1) Antibody	BioLegend	108112; RRID: AB_313349
PerCP/Cyanine5.5 anti-mouse CD45 Antibody	BioLegend	103132; RRID: AB_893340
PE anti-mouse/human CD11b Antibody	BioLegend	101208; RRID: AB_312791
Biotin anti-mouse CD45 Antibody	BioLegend	103104; RRID: AB_312969
Biotin anti-mouse/human CD11b Antibody	BioLegend	101204; RRID: AB_312787
Biotin anti-mouse CD31 Antibody	BioLegend	102504; RRID: AB_312911
Biotin anti-mouse TER-119/Erythroid Cells Antibody	BioLegend	116204; RRID: AB_313705
Biotin anti-mouse CD34 Antibody	BioLegend	119304; RRID: AB_345282
Anti-Glyceraldehyde-3-Phosphate Dehydrogenase Antibody, clone 6C5	Millipore	MAB374; RRID: AB_2107445
Lamin A/C (4C11) Mouse mAb	Cell Signaling Technology	#4777; RRID: AB_10545756
Phospho-Lamin A/C (Ser22) (D2B2E) XP® Rabbit mAb	Cell Signaling Technology	#13448; RRID: AB_2798221
Anti-MMP14 antibody	abcam	ab53712; RRID: AB_881233
Non-phospho (Active) β-catenin (Ser33/37/Thr41) (D13A1) Rabbit mAb	Cell Signaling Technology	#8814; RRID: AB_11127203
Collagen type I, cleavage site, Col 1 - ¾ C	ImmunoGlobe GmbH	0217–050
Purified Mouse Anti-β-catenin	BD Biosciences	610153; RRID: AB_397554
Emerin (D3B9G) XP® Rabbit mAb	Cell Signaling Technology	#30853; RRID: AB_2798996
RUNX2 (D1L7F) Rabbit mAb	Cell Signaling Technology	#12556; RRID: AB_2732805
PPARγ (D8I3Y) Mouse mAb	Cell Signaling Technology	#95128; RRID: AB_2800240
LEAF-purified anti-mouse/rat CD29	Biolegend	102236; RRID: AB_2813928
LEAF-purified Armenian Hamester IgG	Biolegend	400940; RRID: AB_11203529
Purified Rat Anti-Mouse CD29	BD Biosciences	553715; RRID: AB_395001
Anti-Integrin β1 Antibody, clone MB1.2	MilliporeSigma	MAB1997; RRID: AB_2128202
Lamin B1 Polyclonal antibody	Proteintech	12987–1-AP; RRID: AB_2136290
Lamin B2 (E1S1Q) Rabbit mAb	Cell Signaling Technology	#13823; RRID: AB_2798322
Nesprin 1 Rabbit Ab	From Dr. Didier Hodzic	N/A
Nesprin 2 Rabbit Ab	From Dr. Didier Hodzic	N/A
Normal Rabbit IgG	Cell Signaling Technology	#2729; RRID: AB_1031062
Normal Mouse IgG	Cell Signaling Technology	#5415; RRID: AB_10829607
SUN1 Antibody, clone 12.10F	Novus Biologicals	NBP2–59943; RRID: AB_2813863
SUN2 Polyclonal Antibody	ThermoFisher Scientific	27556–1-AP; RRID: AB_2880906
Chemicals, peptides, and recombinant proteins		
Mesenchymal Stem Cell Growth Medium Bulletkit	Lonza	PT3001
Human mesenchymal-XF expansion medium	Sigma-Aldrich	SCM045
Collagenase from *Clostridium histolyticum*	Sigma-Aldrich	C0130
Generic 56 Qgel 3D Matrix-Degradable with RGD peptides	QGEL SA Swiss Biotech	NS56-B
Generic 61 Qgel 3D Matrix- Non-Degradable with RGD peptides	QGEL SA Swiss Biotech	NS61-B

REAGENT or RESOURCE	SOURCE	IDENTIFIER
Recombinant Mouse Wnt-3a Protein	R&D Systems	1324-WN
Batimastat (BB-94)	Selleck Chem	S7155
L-Ascorbic acid 2-phosphate Sesquimagnesium salt hydrate	Sigma-Aldrich	A8960
Dexamethasone	Sigma-Aldrich	D8893
β-Glycerol phosphate disodium salt pentahydrate	Sigma-Aldrich	50020
Indomethacin	Sigma-Aldrich	I7378
3-Isobutyl-1-methylxanthine	Sigma-Aldrich	I7018
Insulin solution human	Sigma-Aldrich	I9278
SIGMAFAST BCIP/NBT	Sigma-Aldrich ThermoFisher	B5655
MagniSort Streptavidin Negative Selection Beads	Scientific	MSNB-6002
Cytochalasin D	Sigma-Aldrich	C2618
Emerin siRNA (m)	Santa Cruz Biotechnology	sc-35297
Control siRNA-A	Santa Cruz Biotechnology	sc-37007
Control siRNA-B	Santa Cruz Biotechnology	sc-44230
Control siRNA-C	Santa Cruz Biotechnology	sc-44231
Deposited Data		
Raw and Analyzed Affymetrix microarray data	This work	N/A
Commercial Kits		
RNeasy Micro Kit (50)	QIAGEN	74004
Power SYBR™ Green PCR Master Mix	ThermoFisher Scientific	4368706
RNeasy Fibrous Tissue Mini Kit (50)	QIAGEN	74704
Human Mesenchymal Stem Cell Nucleofector Kit	Lonza	VAPE-1001
Acid Phosphatase, Leukocyte (TRAP) Kit	Sigma-Aldrich	387A-1KT
Dynabeads Protein G Immunoprecipitation Kit	ThermoFisher Scientific	10007D
PepMute™ siRNA Transfection Reagent	SignaGen Laboatories	SL100566
Cell Lines		
Human Mesenchymal Stem Cells (Bone Marrow)	Sigma-Aldrich	SCC034
Human Mesenchymal Stem Cells (Bone)	Lonza	PT-2501
Experimental Models: Organism/Strains		
Mouse: *Mmp14*$^{+/-}$	From Dr. Kenn Holmbeck	N/A
Mouse: *Lmna*$^{f/f}$	From Dr. Yixian Zheng	N/A
Mouse: *Dermo1-Cre*$^{+/-}$	Jackson Laboratories	Cat # 008712
Mouse: Emd$^{-/-}$	From Dr. Howard J. Worman	N/A
Mouse: Lmna$^{+/-}$	Jackson Laboratories	Cat # 009125
Mouse: Nu/Nu Nude Mouse	Charles River Laboratories	N/A
Oligonucleotides		
5′ ATGGCTCGTGGTACAAGGC 3′	This work	Mouse *Sp7*

REAGENT or RESOURCE	SOURCE	IDENTIFIER
5′ GCAAAGTCAGATGGGTAAGTAGG 3′	This work	Mouse *Sp7*
5′ AGGGCAATGAGGTCACATCC 3′	This work	Mouse *Alp*
5′ GCATCTCGTTATCCGAGTACCAG 3′	This work	Mouse *Alp*
5′ CGGCCCTGAGTCTGACAAA 3′	This work	Mouse *Bglap*
5′ GCCGGAGTCTGTTCACTACCTT 3′	This work	Mouse *Bglap*
5′ GAAATGCCTCCGCTGTTATG 3′	This work	Mouse *Runx2*
5′ AGGTGAAACTCTTGCCTCGTC 3′	This work	Mouse *Runx3*
5′ AGCCGCTTATATGTATCGCTCA 3′	This work	Mouse *Adipoq*
5′ TGCCGTCATAATGATTCTGTTGG 3′	This work	Mouse *Adipoq*
5′ GCGTGGAATTCGATGAAATCA 3′	This work	Mouse *Ap2*
5′ CCCGCCATCTAGGGTTATGA 3′	This work	Mouse *Ap2*
5′ TCGCTGATGCACTGCCTATG 3′	This work	Mouse *Pparg*
5′ GAGAGGTCCACAGAGCTGATT 3′	This work	Mouse *Pparg*
5′ TACCCTTCTTCCGACTGGGGGC 3′	This work	Mouse *Axin2*
5′ TGGTGGTGAACGTGCTTCGTCG 3′	This work	Mouse *Axin2*
5′ CTCAACCCCCGCTGCATAACAA 3′	This work	Mouse *Dkk2*
5′ CCTTGCTTCTGGCTGATGTCCG 3′	This work	Mouse *Dkk2*
5′ TCCACTTTCGGCCCGCCTCT 3′	This work	Mouse *Tcf7*
5′ TATCCCCGGAACCGGCCTCG 3′	This work	Mouse *Tcf7*
5′ TGGCAAAGTGGAGATTGTTGC 3′	This work	Mouse *Gapdh*
5′ GAAATGCCTCCGCTGTTATG 3′	This work	Mouse *Gapdh*
5′ TTATGCTTTGCACTACGTCCCTCCA 3′	This work	Human AXIN2
5′ CGCAACATGGTCAACCCTCAGAC 3′	This work	Human AXIN2
5′ AGTACCCGCTGCAATAATGG 3′	This work	Human DKK2
5′ GAAATGACGAGCACAGCAAA 3′	This work	Human DKK2
5′ CTGACCTCTCTGGCTTCTACTC 3′	This work	Human TCF7
5′ CAGAACCTAGCATCAAGGATGGG 3′	This work	Human TCF7
5′ CGCTCTCTGCTCCTCCTGTT 3′	This work	Human GAPDH
5′ CCATGGTGTCTGAGCGATGT 3′	This work	Human GAPDH
Recombinant DNA		
pBABE-puro-GFP-wt-Lamin A	Addgene	#17662
pMXs-beta-Catenin-S33Y	Addgene	#13371
WT Lamin A minigene	Addgene	#20291
Lamin A (R-527P)-mRFP	Addgene	#124272
pinducer 20 DN-KASHΔPPPL	Addgene	#129280
Software		
ImageJ Prism software (Graphpad Prism 8)	Open Source University of Michigan	https://imagej.nih.gov/ij/ Prism-GraphPad
DAVID Bioinformatics Resource 6.8 Imaris software system	Open Source University of Michigan	https://david.ncifcrf.gov/